
Masters Theses

Student Theses and Dissertations

Summer 2014

Determination of minor and trace elements concentration in kidney stones using elemental analysis techniques

Anjali Srivastava

Follow this and additional works at: https://scholarsmine.mst.edu/masters_theses

 Part of the [Nuclear Engineering Commons](#)

Department:

Recommended Citation

Srivastava, Anjali, "Determination of minor and trace elements concentration in kidney stones using elemental analysis techniques" (2014). *Masters Theses*. 7304.
https://scholarsmine.mst.edu/masters_theses/7304

This thesis is brought to you by Scholars' Mine, a service of the Curtis Laws Wilson Library at Missouri University of Science and Technology. This work is protected by U. S. Copyright Law. Unauthorized use including reproduction for redistribution requires the permission of the copyright holder. For more information, please contact scholarsmine@mst.edu.

DETERMINATION OF MINOR AND TRACE ELEMENTS CONCENTRATION IN
KIDNEY STONES USING ELEMENTAL ANALYSIS TECHNIQUES

by

ANJALI SRIVASTAVA

A THESIS

Presented to the Faculty of the Graduate School of the

MISSOURI UNIVERSITY OF SCIENCE AND TECHNOLOGY

In Partial Fulfillment of the Requirements for the Degree

MASTER OF SCIENCE IN NUCLEAR ENGINEERING

2014

Approved by

Xin Liu, Advisor
Hyoung K. Lee, Co-Advisor (Chairman)
Ayodeji B. Alajo

© 2014

Anjali Srivastava

All Rights Reserved

ABSTRACT

The determination of accurate material composition of a kidney stone is crucial for understanding the formation of the kidney stone as well as for preventive therapeutic strategies. Radiations probing instrumental activation analysis techniques are excellent tools for identification of involved materials present in the kidney stone. The X-ray fluorescence (XRF) and neutron activation analysis (NAA) experiments were performed and different kidney stones were analyzed. The interactions of X-ray photons and neutrons with matter are complementary in nature, resulting in distinctly different materials detection. This is the first approach to utilize combined X-ray fluorescence and neutron activation analysis for a comprehensive analysis of the kidney stones. Presently, experimental studies in conjunction with analytical techniques were used to determine the exact composition of the kidney stone. The use of open source program Python Multi-Channel Analyzer was utilized to unfold the XRF spectrum. A new type of experimental set-up was developed and utilized for XRF and NAA analysis of the kidney stone. To verify the experimental results with analytical calculation, several sets of kidney stones were analyzed using XRF and NAA technique. The elements which were identified from XRF technique are Br, Cu, Ga, Ge, Mo, Nb, Ni, Rb, Se, Sr, Y, Zr. And, by using Neutron Activation Analysis (NAA) are Au, Br, Ca, Er, Hg, I, K, Na, Pm, Sb, Sc, Sm, Tb, Yb, Zn. This thesis presents a new approach for exact detection of accurate material composition of kidney stone materials using XRF and NAA instrumental activation analysis techniques.

ACKNOWLEDGMENTS

I would like to express my deepest sense of gratitude to my advisor Dr. Xin Liu, who offered his continuous advice and support throughout the course of this research. I thank him for the systematic guidance and great effort he put to specialize me in the field of the field of nuclear engineering. I highly appreciate Dr. Liu's guidance and help while I was working on the determination of minor and trace elements in kidney stone using X-ray fluorescence and neutron activation analysis at Missouri University of Science & Technology. I am highly thankful to my co-advisor Dr. Hyoung Koo Lee to provide me solid knowledge and guidance on the subject matter. I appreciate the help of Dr. Ayodeji Alajo for providing advanced knowledge in the field of nuclear engineering and sharing his valuable experiences for a progressive research. I am highly thankful to colleagues at Mayo Clinic to provide support and help in acquiring the kidney stones. I am thankful to MSTR staff; Bill Bonzer, Craig Reisner and Raymond Kendrick for assistance with the neutron activation experiments. I am greatly thankful to my husband Dr. Vaibhav Sinha for his constant help, support and encouragement to pursue my research and academics with great motivation.

TABLE OF CONTENTS

	Page
ABSTRACT	iii
ACKNOWLEDGMENTS	iv
LIST OF ILLUSTRATIONS	vii
LIST OF TABLES	ix
NOMENCLATURE	x
SECTION	
1. INTRODUCTION.....	1
1.1 RADIATION PROBING TECHNIQUES AND KIDNEY STONE ANALYSIS	1
1.2. X-RAY FLUORESCENCE.....	1
1.2.1. Matrix Effects	4
1.2.2. Sherman Equation	5
1.2.3. Fundamental Parameter Method.....	6
1.2.4. Calculation of Concentration	6
1.3. INTERACTION OF PHOTONS WITH MATTER	8
1.3.1. Photoelectric Absorption	8
1.3.2. Characteristic X-rays.....	10
1.3.3. Auger Electrons	11
1.3.4. Fluorescence Yield.....	12
1.3.5. Compton Scattering.....	13
1.3.6. Pair Production	16
1.4. PHOTON ATTENUATION IN KIDNEY STONE.....	17

1.5. NEUTRON ACTIVATION ANALYSIS	18
1.5.1. Theory and Methodology	18
1.5.2. Neutron Energy Distribution	21
1.5.3. Sensitivities Dependence.....	22
2. DESCRIPTION OF INSTRUMENTATION SYSTEMS	23
2.1. X-RAY FLUORESCENCE SYSTEM.....	23
2.2. NEUTRON ACTIVATION EXPERIMENTS	24
2.3. EXPERIMENTAL SET-UP REQUIREMENTS AND SAMPLE PREPARATION.....	26
2.4. DETECTOR SET-UP	28
2.5. SPECTRUM ANALYSIS	29
3. ANALYSIS AND IDENTIFICATION OF ELEMENTS.....	31
3.1. X-RAY FLUORESCENCE.....	31
3.1.1. Concentration Calculation for XRF Measurements.....	36
3.2. NEUTRON ACTIVATION ANALYSIS	37
3.2.1. Concentration Calculation for NAA Measurements.....	43
4. DISCUSSION AND CONCLUSION	45
APPENDIX.....	47
BIBLIOGRAPHY	50
VITA	52

LIST OF ILLUSTRATIONS

Figure	Page
1.1. Energy Dispersive X-ray Fluorescence Sepctrum with Element Concentration	2
1.2. Schematic of X-ray Fluorescence in an Atom.....	4
1.3. Photoelectric Absorption Process	9
1.4. Single Peak at a Total Electron Energy Corresponding to the Energy of the Incident X-rays	10
1.5. K_{α} Characteristic X-ray Emission following Photoelectric Absorption	11
1.6. Auger Electron Emission following Photoelectric Absorption	12
1.7. Fluorescence Yield for K and L Electrons	13
1.8. Schematic of Compton Scattering	14
1.9. Compton Scattering	14
1.10. The Electron Energy Distribution for Compton Continuum.....	15
1.11. Schematic of Pair Production	16
1.12. Plot of Charged Particle KE by the Incident X-ray Energy	17
1.13. Illustration of the NAA Method	19
1.14. Experimental Setup for DGNAA at MST Reactor	20
1.15. Relative Neutron Flux vs. Neutron Energy	21
2.1. Experimental Setup for XRF Studies on Kidney Stone	23
2.2. Experimental Setup of NAA Method	25
2.3. Schematic of Germanium Semiconductor Detector	28
2.4. Schematic of Electronic System for Semiconductor Detector	29
2.5. Flowchart for Gamma ray Spectrum Analysis	30

3.1. Description of XRF Method to Determine the Elements and their Concentration in the Kidney Stones	32
3.2. XRF Spectrum of the Brushite Kidney Stone	33
3.3. XRF Spectrum of the Apatite Kidney Stone	33
3.4. XRF Spectrum of the Calcium Oxalate Monohydrate Kidney Stone Sample 1	34
3.5. XRF Spectrum of the Calcium Oxalate Monohydrate Kidney Stone Sample 2	34
3.6. XRF Spectrum of the Cystine Kidney Stone.....	35
3.7. XRF Spectrum of the Struvite Kidney Stone	35
3.8. XRF Spectrum of the Uric Acid Kidney Stone	36
3.9. Description of NAA Method to Determine the Elements and their Concentration in the Kidney Stones	38
3.10. Analysis of Apatite Kidney Stone using NAA Method with 3 hrs Counting Time	39
3.11. Analysis of Apatite Kidney Stone using NAA Method with 8 hrs Counting Time	39
3.12. Analysis of COM Kidney Stone using NAA Method with 3 hrs Counting Time	40
3.13. Analysis of COM Kidney Stone using NAA Method with 8 hrs Counting Time	40
3.14. Analysis of Struvite Kidney Stone using NAA Method with 3 hrs Counting Time	41
3.15. Analysis of Struvite Kidney Stone using NAA Method with 8 hrs Counting Time	41
3.16. Analysis of Uric Acid Kidney Stone using NAA Method with 3 hrs Counting Time	42
3.17. Analysis of Uric Acid Kidney Stone using NAA Method with 8 hrs Counting Time	42

LIST OF TABLES

Table	Page
1.1. Estimated Detection Limits for INAA using Decay Gamma Rays..	22
2.1. Source and Detector Description of XRF Instrumentation System.....	24
2.2. Source and Detector Description of NAA Instrumentation System.	26
2.3. Description of Kidney Stones.....	27
3.1. Relative Concentrations of Kidney Stones from XRF Measurement.	37
3.2. Relative Concentrations of Kidney Stones from NAA Measurement for 3 Hrs Counting Times	43
3.3. Relative Concentrations of Kidney Stones from NAA Measurement for 8 Hrs Counting Times	44

NOMENCLATURE

Symbol	Description
MSTR	Missouri University of Science & Technology Nuclear Reactor
XRF	X-ray Fluorescence
NAA	Neutron Activation Analysis
INAA	Instrumentation Neutron Activation Analysis
PGNAA	Prompt Gamma Neutron Activation Analysis
DGNAA	Delayed Gamma Neutron Activation Analysis
EDXRF	Energy Dispersive X-ray Fluorescence
PyMCA	Python Multi-Channel Analyzer
FPM	Fundamental Parameter Method
BE	Binding Energy
PE	Photoelectric Effect
CS	Compton Scattering
PP	Pair Production
COM	Calcium Oxalate Monohydrate
CS	Change in Coupler Angle

1. INTRODUCTION

1.1. RADIATION PROBING TECHNIQUES AND KIDNEY STONE ANALYSIS

Kidney stone is one of the most common diseases expected to affect in a person life time. A study suggests that 1 in 11 people suffer from a kidney stone disease in the United States [1]. The main factors contribute to the formation of a kidney stone are age, sex, occupation, social class, climate and dietary habits. Kidney stone is a crystal aggregation formed in the kidney from super saturation of urine with salts. Therefore, formation of different type of kidney stones depend on the urinary pH and type of salt constituents involved in such case. The formation of stone primarily depends on major constituents. However, knowledge of minor and trace elements is also important for treatment and development of medicines for kidney stones. Radiation probing elemental analysis techniques provides an excellent tool of nondestructive examination of a given sample for qualitative and quantitative information. Furthermore, Energy Dispersive X-ray Fluorescence (EDXRF), X-ray Diffraction (XRD), Rutherford Back Scattering (RBS), Proton Back Scattering (PBS) and Instrumental Neutron Activation Analysis (INAA) are popular techniques for determination of minor and trace elements in the kidney stone.

1.2. X-RAY FLUORESCENCE

The widespread use of X-ray Fluorescence (XRF) as a versatile tool for the quantitative and qualitative determination of major, minor and trace elements in the samples of interest can be found in industry, research and medical applications. Basically, X-ray Fluorescence (XRF) Spectroscopy measures the intensity of emitted X-ray from a

sample in terms of energy or wavelength. The energies of intensity are characteristic of atoms of the sample. This observed intensity for a given atoms represents the amount of that particular atoms present in the sample. Therefore, XRF provides qualitative and quantitative data for involved atoms of the elements in the sample. In other words, qualitative approach provides information of involved elements in the sample by identifying atoms associated with the observed characteristics lines of the corresponding atom (see Fig. 1.1).

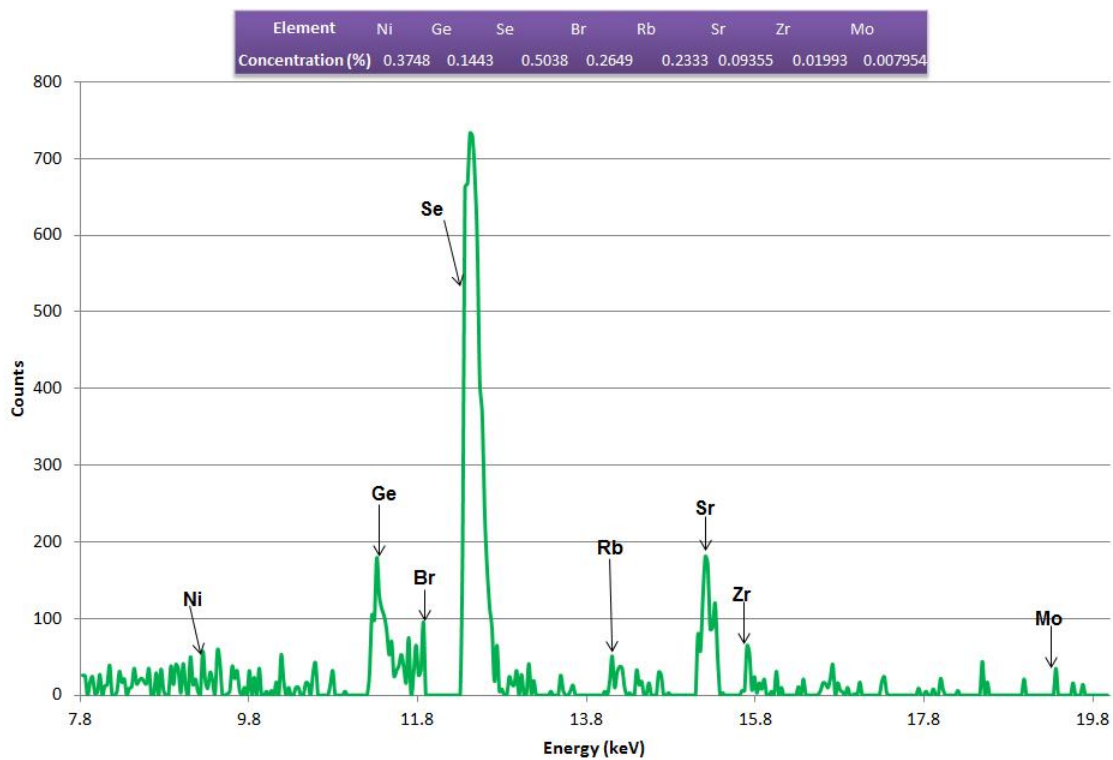


Figure 1.1. Energy Dispersive X-ray Fluorescence Spectrum with Element Concentration

Furthermore, quantitative approach allows determining the amount of each involved atom present in the sample utilizing the intensity of characteristics lines of the

corresponding atom. There are variety of instrumentation can be utilized for X-ray fluorescence spectroscopy. This instrumentation can be classified in two different categories of Wavelength Dispersive and Energy Dispersive spectroscopy, depending on the nature of measurements. As name suggests, in wavelength dispersive spectroscopy, only X-ray intensity as a function of wavelength will be utilized for analysis. Similarly, X-ray intensity as a function of energy can be utilized for spectrum analysis. In this research Energy Dispersive X-ray Fluorescence was utilized for the analysis of kidney stones. It is also important to mention that creation of inner orbital vacancy by different methods is also an important aspect of the XRF spectrometry instrumentation system. Mainly, utilization of high energy X-ray, high energy electrons and proton beams are the methods to bombard the sample. The interaction of photon beam with sample experiences a photon absorption interaction. On the other hand, electron and proton beams experience a Coulomb interaction with the sample. Different types of radiation sources can be used to generate the radiation beam i.e. X-ray tube can produce high energy x-rays but this beam will be polychromatic in nature, radionuclide sources can produce low power monochromatic beam.

In wavelength dispersive spectrometry, Bragg's law and a crystal is used to analyze the wavelength which enters to a detector. A discriminator is applied in this type of arrangements to discard the undesired orders of Bragg reflections. The different analyzing crystals with different Bragg d-spacing can be utilized for wavelength sensitivity of the desired system.

On the other hand, in energy dispersive spectrometry, a solid state detector and a multi-channel analyzer is used to measure the X-ray intensity as a function of energy.

In XRF, the materials get exposed to X-rays or to gamma rays results in the ionization of the atom. The ionization of the atom causes the ejection of one or more electron from the atom, which makes the electronic structure of the atom unstable. In this process, the electron from the higher orbitals falls into lower orbital to fill the hole. Consequently, energy is released in the form of the photon which is equal to the difference of the energy of the involved orbitals (see Fig. 1.2). This emitted radiation and energy is unique to the material involved and can be used to identify different elements and their concentrations in a sample.

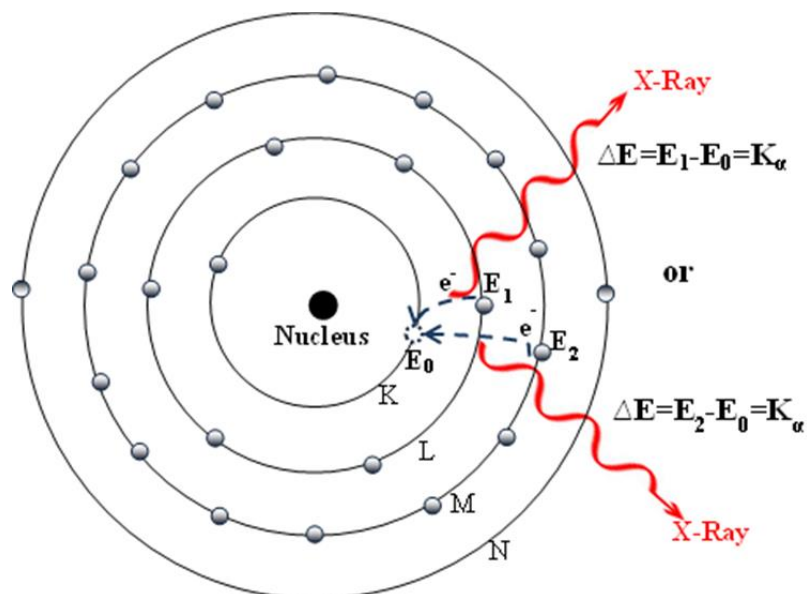


Figure 1.2. Schematic of X-ray Fluorescence in an Atom

1.2.1. Matrix Effects. The primary radiation beam interacts with the sample and get absorbed. Thereafter, a fluoresced X-ray is emitted from an atom and it is also absorbed by the detection system. The fluoresced X-ray may enhance the intensity of

lower energy X-rays. In short, the absorption of primary radiation, and absorption and enhancement of characteristics line is collectively known as matrix effects.

As earlier mentioned that the intensity of the emitted radiation is related to the concentration of the associated element. It is important to mention that to a quantitative relationship between element concentration and characteristics X-ray needs to be established. The below general equation given by Hamos [2], can be utilized for expressing the above discussed relationship.

$$R_i = C_i K_i \quad (1)$$

Where R_i is the ratio between the measured x-ray intensity of element i in an unknown sample and the x-ray intensity measured for a sample of element i . The constant K_i is a function of the composition of the sample, the mass absorption coefficients of sample constituents, and the measurement geometry. The above equation provides an empirical method of determining element concentrations from measured counts.

1.2.2. Sherman Equation. The use of X-ray fluorescence for the determination of unknown elements in the sample became popular after the discovery of XRF. Therefore, to better describe X-ray absorption and enhancement, Sherman [3, 4] provided a more specific equation for the relationship between the fluoresced x-ray intensity and a multi element sample exposed to a monochromatic beam of energy E for primary absorption.

$$I_i = \frac{S\Omega}{4\pi \sin\psi_1} \frac{C_i g_i \kappa(E_i, I_i) \mu_i(E)}{\frac{\mu(E)}{\sin\psi_1} + \frac{\mu(E_i)}{\sin\psi_2}} \quad (2)$$

Also note that,

$$\mu(E) = \sum_j C_j \mu_j(E) \quad (3)$$

Where, I_i is Intensity of observed characteristic line of element i , E is Energy of incident radiation, E_i is Energy of the characteristic line of element i being measured, S is Irradiated surface area of specimen, C_i is Concentration of element i in the specimen, g_i is Proportionality constant for characteristic line of element i , ψ_1 is Angle between the specimen surface and the incident x-rays, ψ_2 is Angle between the specimen surface and the detector, Ω is Solid angle subtended by the detector, $\kappa(E_i, I_i)$ is Response of instrument at energy E_i of characteristic line energy of element i , $\mu_i(E)$ is Mass absorption coefficient of element i at incident energy E , $\mu(E)$ is Total absorption coefficient of specimen at incident energy E , $\mu(E_i)$ is Total absorption coefficient of specimen at characteristic line energy of element i .

1.2.3. Fundamental Parameter Method. The above description of Sherman's equation represents the intensity of a characteristic X-ray fluoresced from an element contained in a sample of known composition. The information of determined concentration of elements can be utilized to calculate the composition of a sample utilizing measured set of intensities. This direct use of Sherman's equation is known as the Fundamental Parameter method. Furthermore, in this method, the effect of instrument and measurement geometry in the calculation can be removed by utilizing characteristics line intensities of known composition. Theoretically, this equation applicable for all absorption and enhancement therefore a standard is required for each element in the sample. It should be noted that this required standard must account for reflection from the surface of the sample.

1.2.4. Calculation of Concentration. The general and basic expression used in XRF analysis for converting measured net intensities into concentrations is given by [5]

$$C_i = K_i \times I_i \times M_i \quad (4)$$

Where, C_i = Concentration of the element in the sample

K_i = Calibration factor

I_i = Measured net intensity of i

M_i = Factor correcting the effect of the sample matrix composition on intensity i

There are numerous established methods to perform quantification in XRF spectrometry. These methods can be broadly classified into two types; empirical and theoretical methods. The empirical and theoretical methods can be further sub-categorized depending on the factors such as sample preparation, applied radiation intensity and resulting measurements. In short, the intensity of the emitted radiation is always related to the concentration of the elements and different procedures can be adopted or proposed to perform the quantitative analysis of the sample. In addition, it has been found that methods demonstrated by Hamos and Sherman have been frequently applied in the researched literature. The “Fundamental Parameter Method” is an example of such method which is the direct use of the Sherman’s equation. Moreover, advancement in computational techniques led to the development of commercial and open source programs i.e. AXIAL and PyMCA for quantitative and qualitative analysis of the XRF spectrometry data. The program algorithms mainly rely on the spectrum fitting techniques and thereupon procedures. In this research, efforts were being made to utilize an open source program PyMCA to determine the elements of different types of kidney stones and their concentrations using XRF spectrometry. This is the first approach to perform such analysis and it will facilitate the inexpensive measurements in

determining the elements of the kidney stones and their concentrations. To establish a consistency in measurements several kidney stone were analyzed. To perform the XRF experiments a gamma source Cd-109 of 1 μ Ci was used for the photo excitation of the kidney stone. Ortec GLP series (> 3 keV) detector was used for the measurements. The energy spectrum was obtained from XRF. The energy peaks of obtained spectrum were then used to analyze the elements using open source PyMCA program. The results can be effectively utilized for preventive therapeutic studies and development of new medicines for treatment of kidney stones.

1.3. INTERACTION OF PHOTONS WITH MATTER

Photons are a form of electromagnetic radiation with no mass, no charge and have a velocity equivalent to speed of light. Since, photons are electrically neutral so they do not lose energy through interaction with atomic electrons like charged particles. Photon travels at considerable distance and interact with atomic electrons resulting in partial or total photon energy transfer to electron energy. The resulting electrons then deposit the energy in the medium. Photons are more penetrating compared to charged particles for the same energy [6].

1.3.1. Photoelectric Absorption. In photoelectric absorption, photons get completely absorbed by the matter, and eject an orbital electron (see Fig.1.3). The photoelectron gets emitted by one of the bound shell (K, L, M or N) of an atom. The energy of the photon must be equal to the photoelectron for photoelectric absorption to occur. In other words, the photoelectric effect occurs between a photon and a bound atomic electron. The photoelectron is ejected with a kinetic energy equivalent to the

difference between the initial photon energy and the binding energy of the electron. The kinetic energy of the electron can be described by:

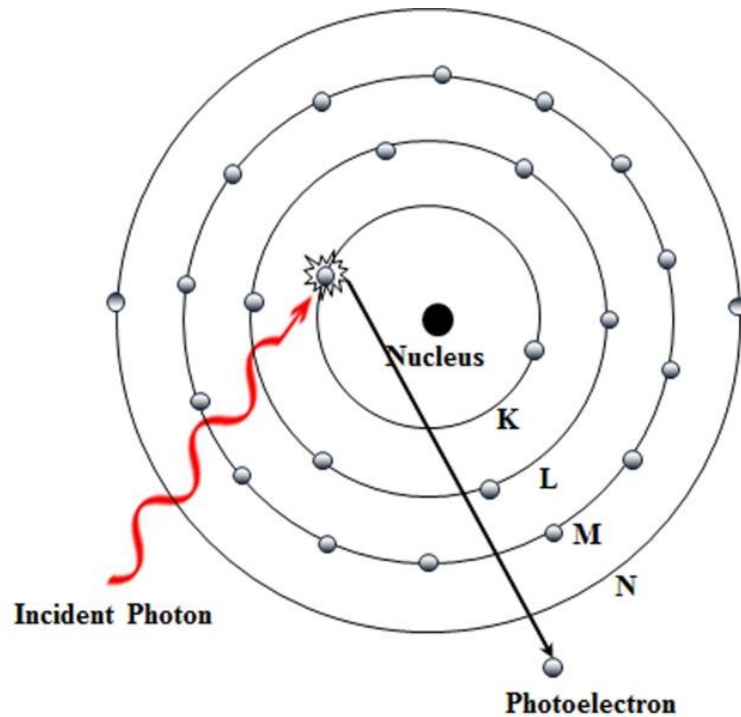


Figure 1.3. Photoelectric Absorption Process [6]

$$E_e = h\nu - BE \quad (5)$$

Where, $h\nu$ = photon energy

$h = 6.626 \times 10^{-34}$ J.s (Planck's Constant)

ν = Frequency of X-ray

BE = binding energy

Photoelectric absorption is the dominant process for photon energies in the order of 50keV. It is also dominant in atoms of the high atomic number materials. It is shown

(see Fig.1.4) that when the total electron kinetic energy is equal to the incident X-ray energy, the differential distribution of electron kinetic energy for a series of photoelectric absorption events will be a simple delta function. [7, 8]



Figure 1.4. Single Peak at a Total Electron Energy Corresponding to the Energy of the Incident X-rays

1.3.2. Characteristic X-rays. The release of energy following electronic transition appears as an X-ray energy which is equal to the difference of the binding energy of the two electron states. A characteristic X-ray produced by an electron from the L shell by filling a vacancy into the K shell is termed as K_{α} . The energy of K_{α} is equal to the difference between the binding energies of K and L shells. Similarly, K_{β} and K_{γ} are equal to the difference between the binding energies of K and L, and M and K shell, respectively. Furthermore, the stable atom has discrete electronic shell and therefore

emits a characteristic fluorescent radiation (see Fig.1.5). This phenomenon is used by energy dispersive X-ray fluorescence for elemental analysis [9, 10].

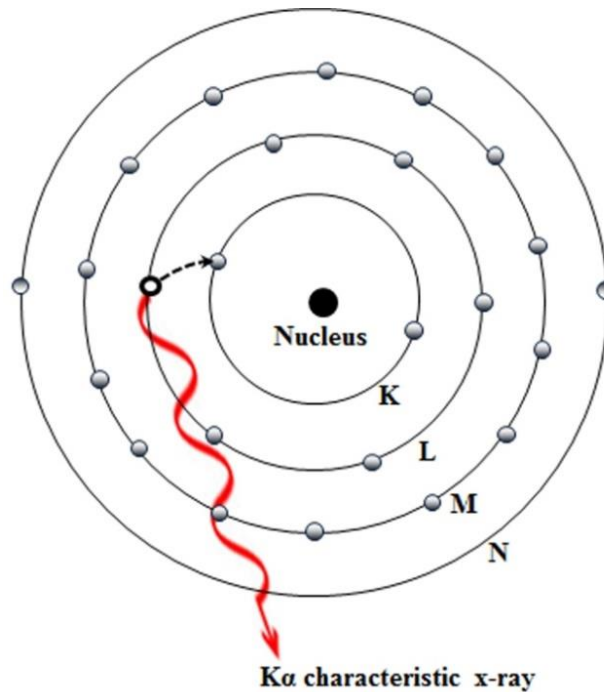


Figure 1.5. K α Characteristic X-ray Emission following Photoelectric Absorption [6]

1.3.3. Auger Electrons. An atom may return back to a stable state after the photoelectric absorption by transferring its excitation energy to an outer shell electron. This ejected electron from orbital known as an Auger electron (see Fig. 1.6). The energy of this Auger electron is equal to the difference of atomic excitation energy and the binding energy of the orbit from where the Auger electron is ejected. The Auger effect is more pronounced in the low atomic number materials than the high atomic number materials [9, 10].

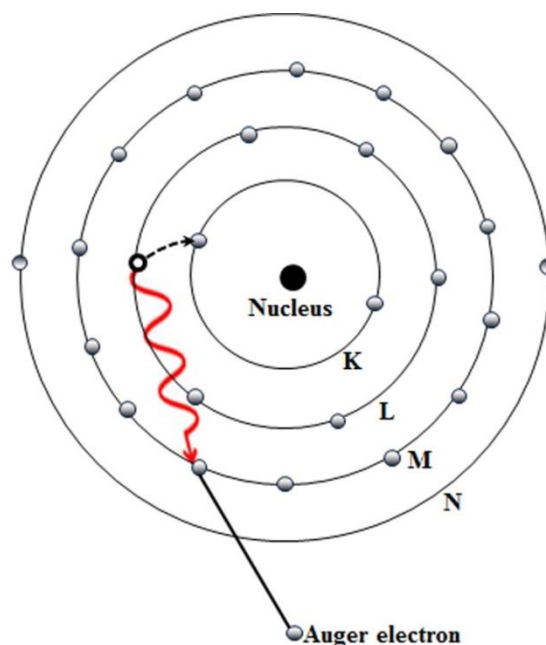


Figure 1.6. Auger Electron Emission following Photoelectric Absorption [6]

1.3.4. Fluorescence Yield. It is clear from above discussion that all incident X-ray photons do not result in fluorescent X-ray emissions and the fraction of characteristic X-ray emission are expressed by the fluorescence yield. It is important to yield high fluorescence for XRF measurements. The emissions of a characteristic X-ray and an electron, both are competing mechanism in atomic de-excitation for photoelectric absorption. Therefore, the fraction of characteristic X-ray emission after the electron shell ionization can be given by the fluorescence yield. For example K shell ionization, the fluorescence yield can be given by the following equation:

$$\omega_k = \frac{n_k}{N_k} \quad (6)$$

Where, n_k is the number of K_α X-rays emitted from the sample and N_k is the number of vacancies created in the K shell. The K-shell fluorescence yield is smaller for light materials and increases sharply for high atomic number materials as fraction of

Auger electron decreases (see Fig.1.7). It is important to note that fluorescent yield of value 1 would be ideal for XRF measurements. Therefore, fluorescent yield plays an important role for counting statistics during measurements.

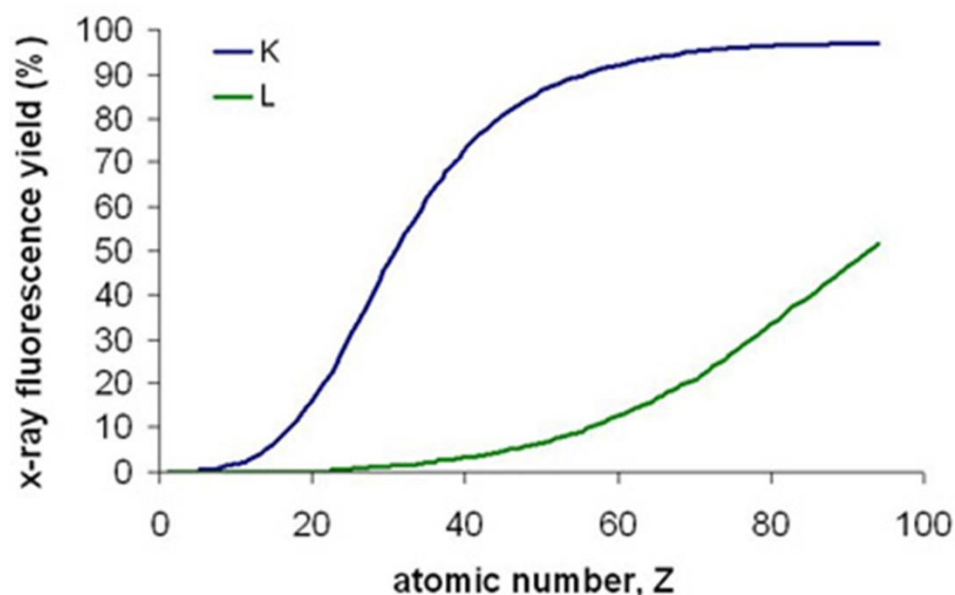


Figure 1.7. Fluorescence Yield for K and L Electrons [11]

1.3.5. Compton Scattering. In Compton Scattering a high-energy photon interacts with a target, which has loosely bound electrons on its outer shell. After the interaction, the photon changes direction and its energy is reduced to an amount that is given off to the electron (see Fig. 1.8, 1.9). Compton scattering occurs between the energy ranges of 100keV to 10MeV. In this process, X-rays rays impinge on the detector, but impart some of its energy to an electron(s). The remaining energy is then converted into a new, lower energy, scattered X-ray. If the incident X-ray has a frequency, ν and is scattered through an angle θ , the kinetic energy of the electron is given by [12, 13]:

$$E_e = h\nu - h\nu' \quad (7)$$

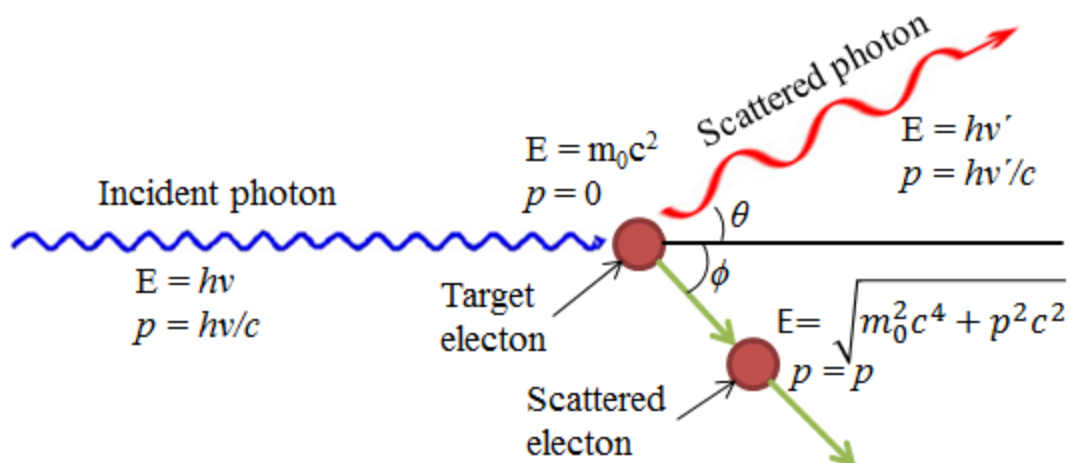


Figure 1.8. Schematic of Compton Scattering [12]

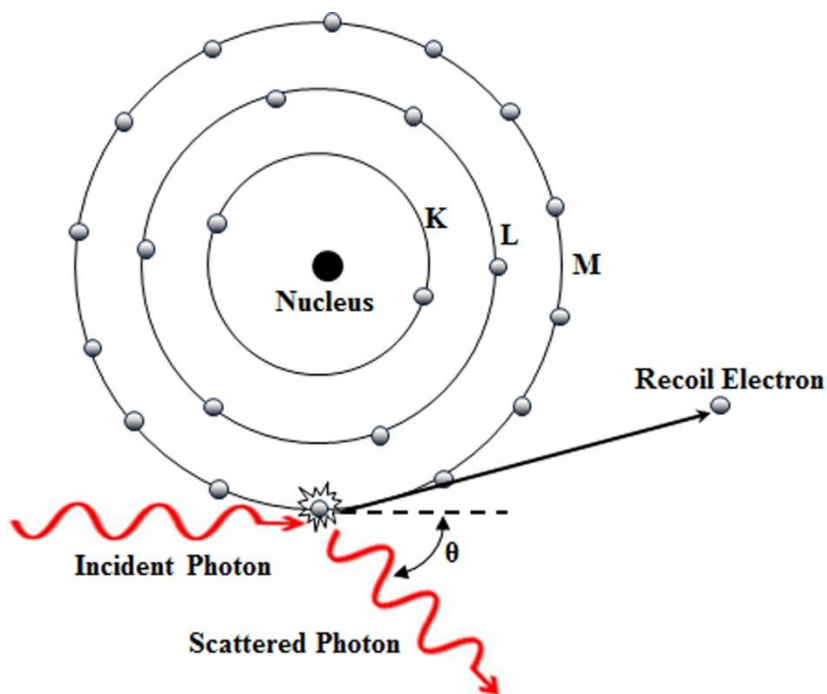


Figure 1.9. Compton Scattering [6]

By the principle of conservation of momentum, the energy of the scattered photon as a function of scattering angle, θ is given by:

$$hv' = \frac{hv}{1 + (1 - \cos\theta) \frac{hv}{c^2 m_0}} \quad (8)$$

Where m_0 is the rest mass of an electron. Thus the kinetic energy transferred to the electron is:

$$E_e = hv - hv' = hv \frac{(1 - \cos\theta) \frac{hv}{c^2 m_0}}{1 + (1 - \cos\theta) \frac{hv}{c^2 m_0}} \quad (9)$$

Between the energy range of 0.5 MeV and 2.5MeV; Compton scattering is the dominant Process, whereby photons transfer their energy to matter. The physical form of the medium through which the X-rays are passing is not very important. It is the electron density, which is related to the bulk density of the medium, which is the important factor. In normal circumstances, all scattering angles will occur in the detector. Therefore, a continuum of energies can be transferred to the electron, ranging from zero up to the maximum value, i.e. when $\theta = \pi$. (see Fig. 1.10) [7]

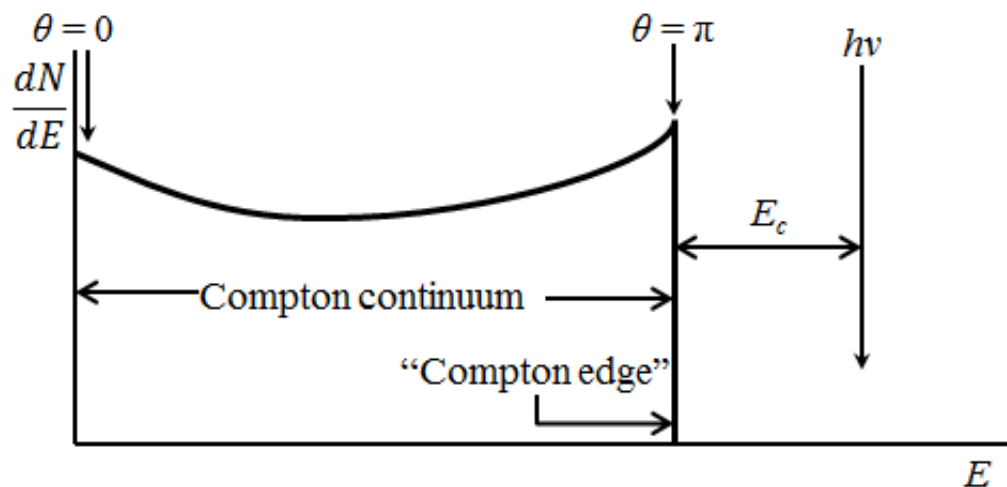


Figure 1.10. The Electron Energy Distribution for Compton Continuum

1.3.6. Pair Production. Pair production takes place with high-energy X-rays where energies greater than 1.02MeV. In this process, the X-ray photon spontaneously transforms into an electron and positron (see Fig. 1.11, 1.12) when it is in the vicinity of the Coulomb force of the nucleus. The excess energy of the rest mass of the electron and positron is transferred into the kinetic energy of the two particles and the recoil of the local nucleus. Typically, both the electron and positron travel very short distances before losing their kinetic energy to the absorbing medium. Thus a spike occurs at an energy corresponding to the initial energy of the X-ray minus the rest mass of the two particles:

$$E_{\text{pair}} = h\nu - 2m_0c^2 \quad (10)$$

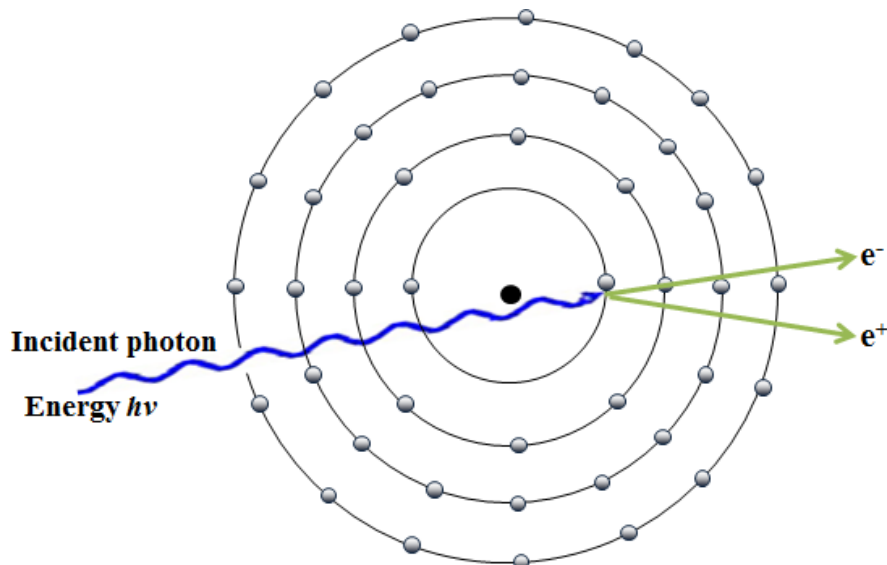


Figure 1.11. Schematic of Pair Production

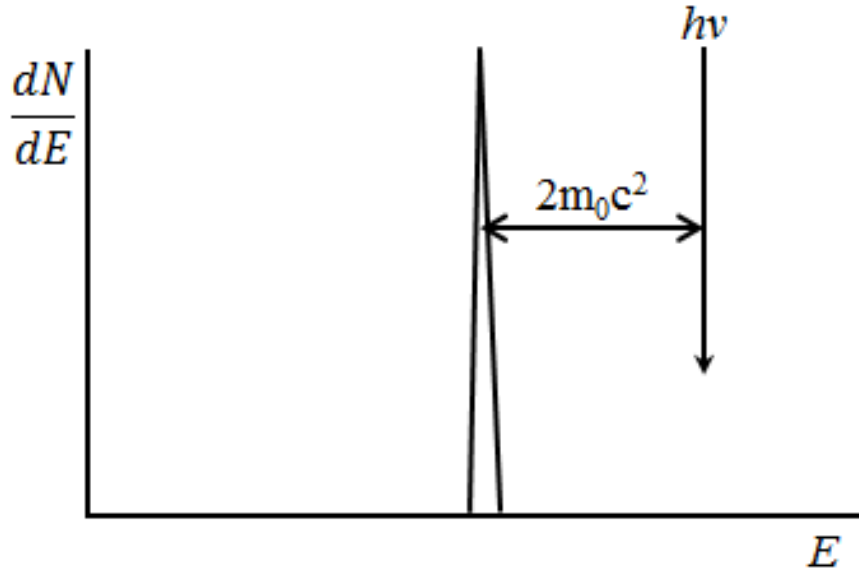


Figure 1.12. Plot of Charged Particle KE by the Incident X-ray Energy

1.4. PHOTON ATTENUATION IN KIDNEY STONE

The photon attenuation in the kidney stones can be expressed by that how many photons interact with atomic electrons of the kidney stones. This fraction can be mathematically expressed by the following equation.

$$F = 1 - e^{-\mu_m \rho x} \quad (11)$$

In above equation, μ_m is the mass attenuation coefficient, ρ is the density and x is the thickness of the kidney stones. The mass attenuation coefficient represents the probability of all possible photon interactions in a unit mass. Furthermore, a graph of the mass attenuation coefficient and photon energy can be plotted and then absorption edges can be identified. Based on absorption edges, attenuation characteristics in terms of photoelectric absorption, pair production in nuclear/electron field, coherent/incoherent scattering and total attenuation can be described for a particular sample [10].

1.5. NEUTRON ACTIVATION ANALYSIS

NAA is routinely used worldwide as a referee method to identify trace elements in samples. Neutron Activation Analysis (NAA) is a sensitive multi element analytical technique. It is mainly used for qualitative and quantitative analysis of major, minor and rare elements. NAA was discovered by Hevesy and Levi in 1936 [14]; they found certain elements become highly radioactive after exposure to source of neutrons. In comparison to other spectroscopic techniques, NAA relies on nuclear transitions than electronic transitions. For elemental analysis, NAA offers sensitivities that are superior to other elemental techniques, on the order of parts per billion or better [14-17].

In NAA, sample is irradiated under neutron flux, consequently become radioactive. This radioactive sample becomes stable by emission of one or more gamma rays. Due to the fact, specific gamma ray energy recorded by semiconductor detector; element(s) in the sample corresponding to their gamma energy levels can be identified in an efficient manner. Furthermore, there are other factors that can also be accounted for the detection of the specific elements in the sample; such as specific half-life of radionuclide, prompt gamma ray emission, delayed gamma ray emission or particular form of radionuclide after few/ several hours of irradiation. The main instrumentation system are required to perform NAA is a need of neutron source (MST reactor in our case) to irradiate the sample, semiconductor detector (HPGe detector) to detect gamma rays and comprehensive knowledge of the reactions when neutron interacts with the particular sample. [14-16]

1.5.1. Theory and Methodology. In neutron activation analysis, (see Fig.1.13) sample is initially irradiated under neutron flux to obtain specific gamma ray signature

for a particular element in the provided kidney stone. Furthermore, neutrons interact with the sample via an inelastic collision, a target nucleus absorbs a neutron (uncharged particle) and transforms into a compound nucleus in an excited state. The excitation energy of the compound nucleus depends on the binding energy of the neutron with the nucleus. To attain a stable configuration this excited nucleus de-excites into a more stable configuration through emission of one or more characteristic prompt gamma rays.

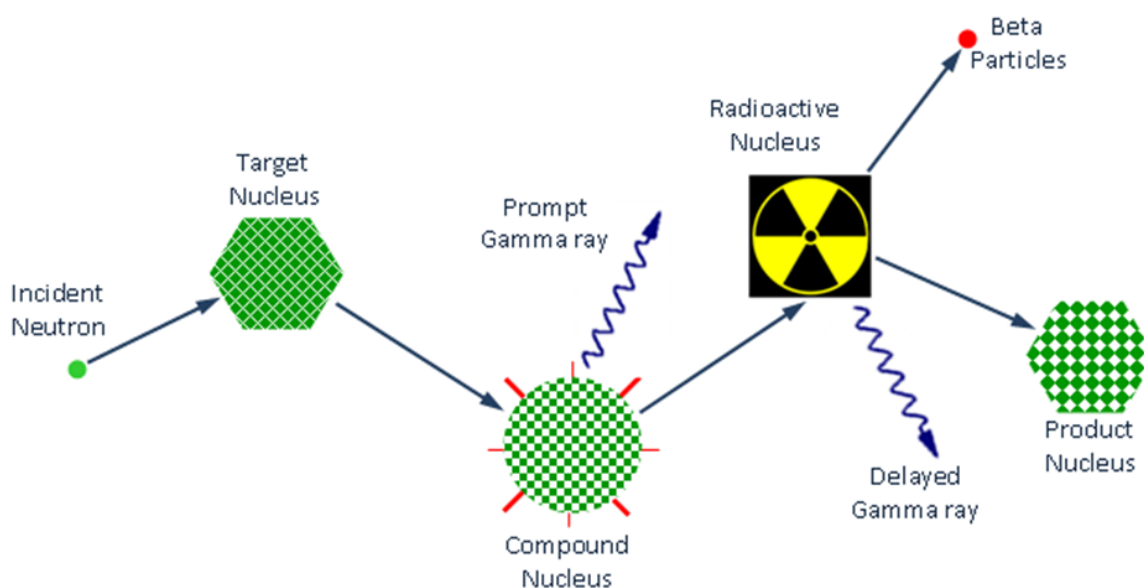


Figure 1.13. Illustration of the NAA Method

In many cases, compound nucleus decays by emission of one or more characteristic delayed gamma rays, but at a much slower rate according to the unique half-life of the radioactive nucleus. In particular, with respect to the counting time of delayed gamma ray on semiconductor detector, NAA can be described into two categories: 1) Prompt Gamma Ray Neutron Activation Analysis, 2) Delayed Gamma Ray

Neutron Activation Analysis. In PGNAA, gamma ray counting takes place during the irradiation or immediately after the irradiation. The PGNAA technique is employed to the elements with extremely high neutron capture cross-sections (B, Cd, Sm, and Gd); these elements decays so rapidly and difficult to measure by DGNAA method. On the other hand, in DGNAA counting takes place after the irradiation and depends on the half-life characteristic of decayed radionuclide. As a result, interference by shorter-lived radionuclide can be removed and provide better sensitivity for a longer lived radionuclide [14-17]. At the MST reactor (see Fig.1.14), NAA analysis has been performed for identification of elements in the kidney stone. In principle, identification of the particular element in a sample was determined by using delayed gamma neutron activation analysis. As explained above, analysis has been performed using DGNAA method. The irradiation time and reactor power was varied (lower to higher) to obtain reliable gamma ray energy spectrum. In addition, counting time (lower to higher), and decay time was also optimized to get the best possible results.

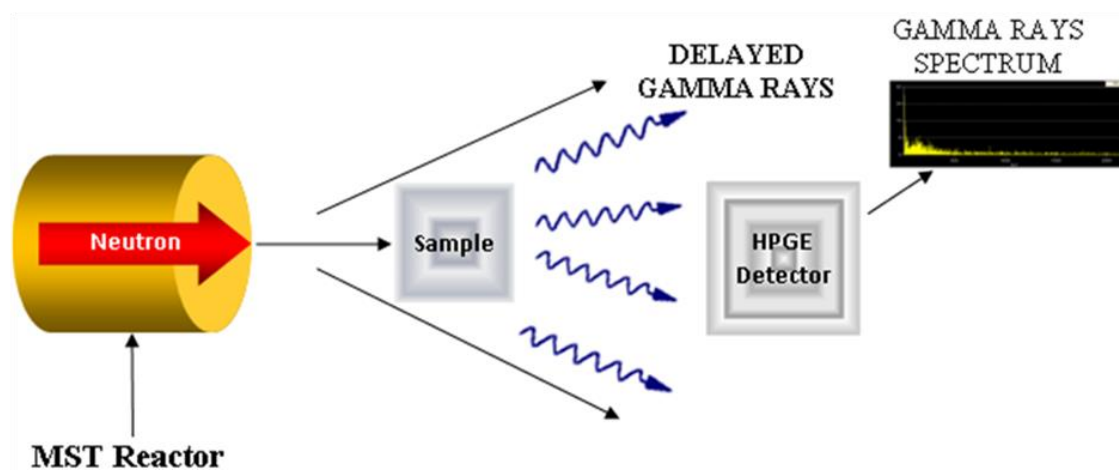


Figure 1.14. Experimental Setup for DGNAA at MST Reactor

1.5.2. Neutron Energy Distribution. In NAA, various types of neutron sources (reactors, accelerators, and radioisotopic neutron emitters) can be used, nuclear reactor with high flux provide the best sensitivity. The neutron energy distributions (see Fig.1.15) are quite broad and consist of three principal components (thermal, epithermal, and fast).

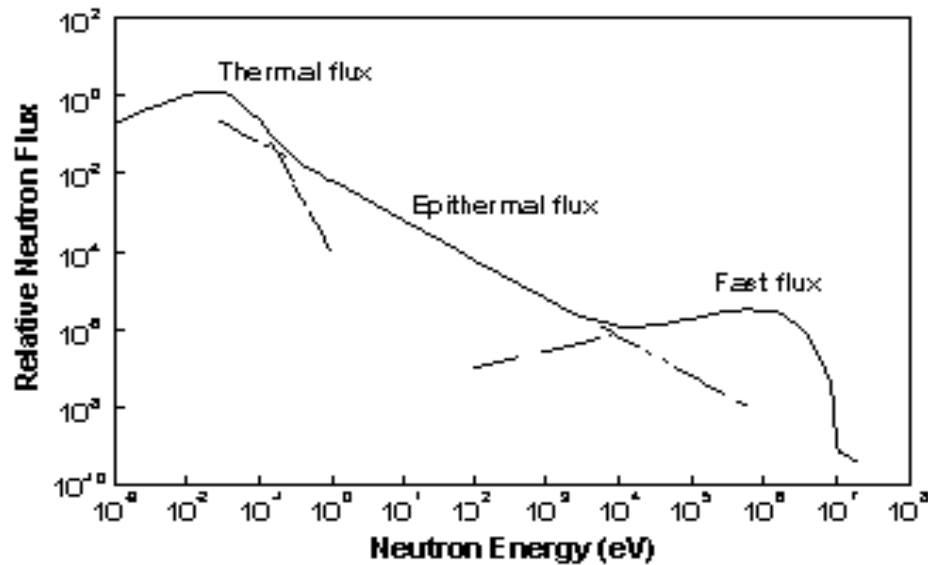


Figure 1.15. Relative Neutron Flux vs. Neutron Energy [14]

- The thermal neutron - low-energy neutrons (energies below 0.5 eV)
- The epithermal neutron component consists of neutrons (energies from 0.5 eV to about 0.5 MeV)
- Thermal and epithermal neutrons induce (n,γ) reactions on target nuclei.
- The fast neutron component of the neutron spectrum (energies above 0.5 MeV)
- Fast neutrons contribute very little to the (n,γ) reaction, but instead induce nuclear

reactions where the ejection of one or more nuclear particles - (n,p), (n,n'), and (n,2n)

In general, a one-megawatt reactor has a peak thermal neutron flux of approximately $1E13$ neutrons per square centimeter per second. [14]

1.5.3. Sensitivities Dependence. The sensitivity of NAA depends on the irradiation parameters (neutron flux, irradiation time and decay time), counting conditions (measurement time, detector efficiency), and nuclear parameters (isotopic abundance, neutron absorption cross sections, half-life, and gamma-ray abundance). “The accuracy of an individual NAA determination usually ranges between 1 to 10 percent of the reported value. (see Table 1.1) lists the approximate sensitivities for determination of elements assuming interference free spectra.”[14]

Table 1.1 Estimated Detection Limits for INAA using Decay Gamma Rays. Assuming Irradiation in a Reactor Neutron Flux of $1 \times 10^{13} \text{ n cm}^{-2} \text{ s}^{-1}$. [14]

Sensitivity (picograms)	Elements
1	Dy, Eu
1–10	In, Lu, Mn
10–100	Au, Ho, Ir, Re, Sm, W
100–1E3	Ag, Ar, As, Br, Cl, Co, Cs, Cu, Er, Ga, Hf, I, La, Sb, Sc, Se, Ta, Tb, Th, Tm, U, V, Yb
1E3–1E4	Al, Ba, Cd, Ce, Cr, Hg, Kr, Gd, Ge, Mo, Na, Nd, Ni, Os, Pd, Rb, Rh, Ru, Sr, Te, Zn, Zr
1E4–1E5	Bi, Ca, K, Mg, P, Pt, Si, Sn, Ti, Tl, Xe, Y
1E5–1E6	F, Fe, Nb, Ne
1E7	Pb, S

2. DESCRIPTION OF INSTRUMENTATION SYSTEMS

2.1. X-RAY FLUORESCENCE SYSTEM

The XRF instrumentation used in this research was consisting of a radiation source to excite the kidney stone, a HPGe detector to collect the fluorescent X-rays and associate electronics to analyze the spectrum (see Fig. 2.1 and Table 2.1). The Cd-109 source was specifically chosen for its stability and small size for continuous and monochromatic beam. The Cd-109 emits energy at 88 keV (4%), 25 keV (14 %), 22 keV (85%) which is useful to detect light atomic number elements in the kidney stones. Furthermore, Cd-109 can detect characteristic K-line of elements from Iron (Fe) to Molybdenum (Mo) and characteristic L-line of elements from Ytterbium (Yb) to Plutonium (Pb).

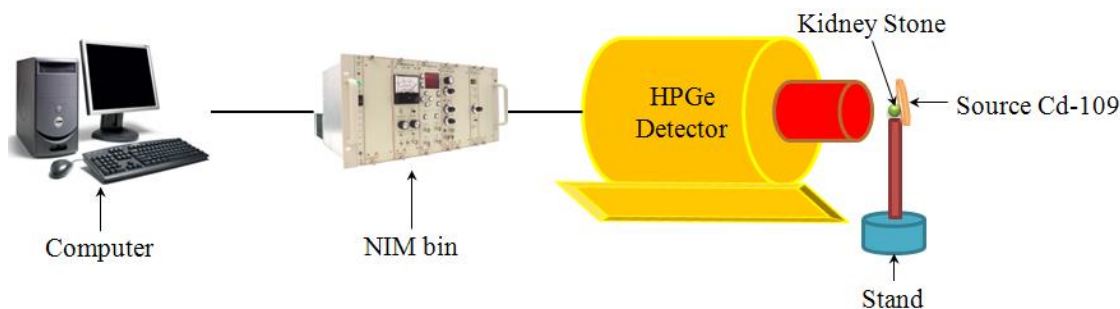




Figure 2.1. Experimental Setup for XRF Studies on Kidney Stone [18]

Table 2.1 Source and Detector Description of XRF Instrumentation System [18]

SOURCE		
	Isotope	Cd109
	Activity	1 µCi
	Half-life	453 days
	Emissions	Gamma
	Energies (MeV)	0.088 (4%), 0.025 (14 %), 0.022 (85%)
HPGe DETECTOR		
	Model No.	GLP-16195/10P4
	Detector Diameter	16 mm
	Detector Length	10 mm
	End Cap to Detector	7 mm
	Dead Layers (Germanium)	0.3 µm
	Window Thickness (Beryllium)	0.127 mm
	Operating Bias (Recommended)	- 2000V
	Resolution (FWHM) at 5.9 keV, 55Fe	204 eV
	Resolution(FWHM) at 122 keV, 57Co	506 eV

2.2. NEUTRON ACTIVATION EXPERIMENTS

The neutron activation analysis experiments require a neutron source to irradiate the kidney stones. In general, a neutron generator or a nuclear reactor can be utilized to perform such experiments. In this research, MST nuclear reactor (see Fig. 2.2) was utilized to perform NAA on the kidney stones. Furthermore, utilization of nuclear reactor will also be more effective and efficient, because high thermal neutron flux can be achieved in this case. In addition, most elements use to have high thermal absorption cross-section which will also help in detection of elements in the irradiated kidney stone. The thermal neutron absorption cross-section represents the probability of neutron capture in thermal region.

The MSTR is an open-pool type research reactor which has maximum power of 200 kW. The nuclear reactor has a number of facilities which can be used for sample irradiation and experiments. These include the thermal column, beam port, pneumatic sample transfer system, sample rotor assembly, core access and isotope production elements, and void tubes. In this research, the pneumatic transfer (rabbit) system was used to rapidly transfer kidney samples to and from the reactor core. The kidney stone samples were irradiated at 100 kW power for 3 hours. The irradiated kidney stone samples were then counted on the HPGe detector (see Table 2.2).

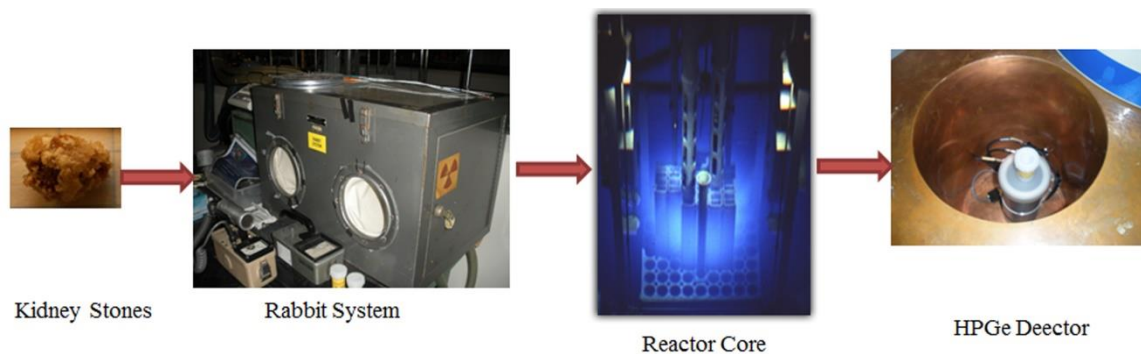




Figure 2.2. Experimental Setup of NAA Method

Table 2.2. Source and Detector Description of NAA Instrumentation System

SOURCE		
	Power	1-200 kW
	Flux	$4.3E12 \text{ ncm}^{-2}\text{s}^{-1}$
HPGe DETECTOR		
	Model No.	BE3825
	Detector Diameter	70 mm
	End Cap to Detector	3.50 inches
	Window Thickness (Carbon Composition)	0.6 mm
	Operating Bias (Recommended)	4000V
	Resolution (FWHM) at 5.9 keV, ^{55}Fe	403 eV
Resolution(FWHM) at 122 keV, ^{57}Co	617 eV	




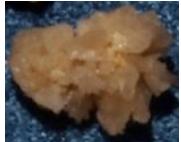



2.3. EXPERIMENTAL SET-UP REQUIREMENTS AND SAMPLE PREPARATION

To perform XRF and NAA experiments on the kidney stones specific set of requirements have been considered. The complete description of kidney stones and their chemical composition are provided in the given table (see Table 2.3). Radiation source for the irradiation of kidney stone was selected based on the energy range requirement and detector properties. The kidney stone samples were dried at room temperature for two weeks. The drying process was conducted in a controlled environment. Once the drying period was complete, the sample was put into a polyethylene vial. Gloves were worn at all times while the sample or vial was being handled. These efforts were meant to help avoid unnecessary contamination. Furthermore, for NAA experiments the dried

kidney stone samples were converted into a powdered form using a pestle and mortar.

The powdered kidney stones were then transferred to a plastic vial for NAA experiments.

Table 2.3 Description of Kidney Stones

APATITE KIDNEY STONE		
	Composition	$\text{Ca}_5(\text{PO}_4)_3(\text{F}, \text{Cl}, \text{OH})$
	Density (g/cm^3)	3.19
	Mass (g)	0.11690
BRUSHITE KIDNEY STONE		
	Composition	$\text{CaHPO}_4 \cdot 2\text{H}_2\text{O}$
	Density (g/cm^3)	2.328
	Mass (g)	0.05397
CALCIUM OXALATE MONOHYDRATE (1) KIDNEY STONE		
	Composition	$\text{C}_2\text{H}_2\text{CaO}_5$
	Density (g/cm^3)	2.12
	Mass (g)	0.12555
CALCIUM OXALATE MONOHYDRATE (2) KIDNEY STONE		
	Composition	$\text{C}_2\text{H}_2\text{CaO}_5$
	Density (g/cm^3)	2.12
	Mass (g)	0.03888
CRYSTINE KIDNEY STONE		
	Composition	$\text{C}_6\text{H}_{12}\text{N}_2\text{O}_4\text{S}_2$
	Density (g/cm^3)	1.48
	Mass (g)	0.08234
STRUVITE KIDNEY STONE		
	Composition	$\text{NH}_4\text{MgPO}_4 \cdot 6\text{H}_2\text{O}$
	Density (g/cm^3)	1.7
	Mass (g)	0.14770
URIC ACID KIDNEY STONE		
	Composition	$\text{C}_5\text{H}_4\text{N}_4\text{O}_3$
	Density (g/cm^3)	1.89
	Mass (g)	0.14209

2.4. DETECTOR SET-UP

Photons can interact with a germanium crystal in various ways. However, in detector operation three main interaction processes (photoelectric absorption, Compton scattering and pair production) are normally considered. In all three cases generation of free electrons take place. These electrons are slowed down on their path through the matter and they create electron-ion or electron-hole pair. In a photon detector, one makes use of these charged pair either to detect the passage of a photon or to determine its energy by measuring the quantity of charge produced (see Fig. 2.3) [19].

The operation of a detector involves:

- First, the conversion of the photon energy to kinetic energy of electrons (and positrons) by following interaction process; photoelectric absorption, Compton scattering or pair production.
- Second, the production of electron-ion pairs, electron-hole pairs or excited molecular states by these electrons.
- Third, Collection of ions and measurement of the charge carriers. [19]

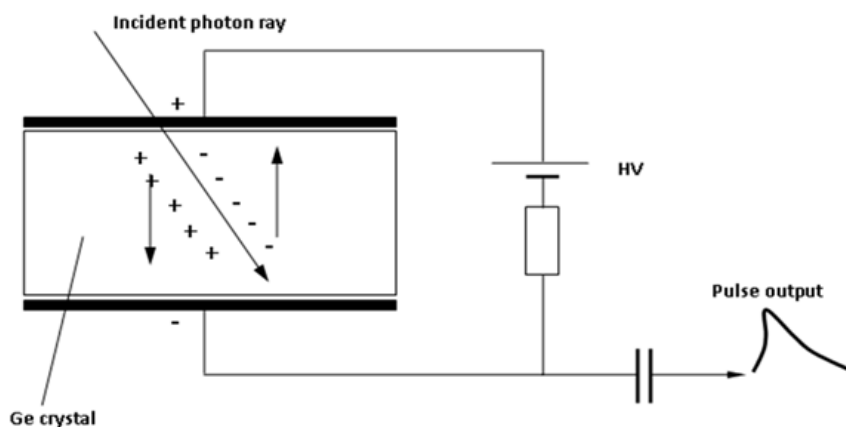


Figure 2.3. Schematic of Germanium Semiconductor Detector [8, 19]

Under the influence of an electric field (as Germanium detector is attached to voltage supply), electrons and holes travel to the electrodes, where they result in a pulse that can be measured in an outer circuit (see Fig. 2.4). As the amount of energy required to create an electron-hole pair is known, and is independent of the energy of the incident radiation, measuring the number of electron-hole pairs allows the energy of the incident radiation to be found [8].

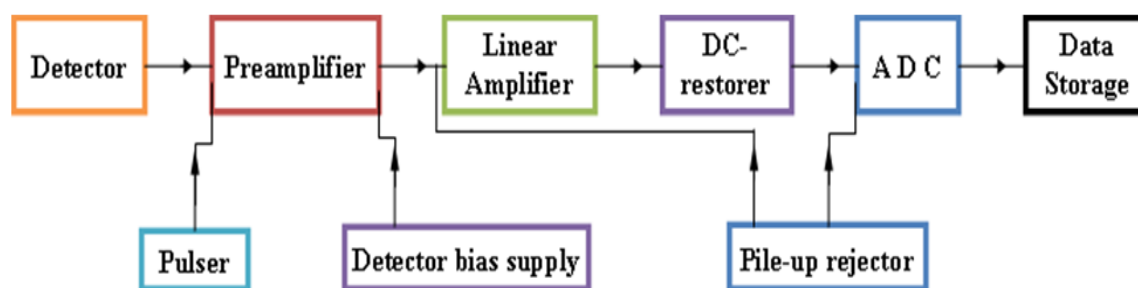


Figure 2.4. Schematic of Electronic System for Semiconductor Detector

2.5. SPECTRUM ANALYSIS

The objective of spectrum analysis (see Fig 2.5) is to identify the photon energy peaks and to determine the activity of the irradiated samples using gamma ray spectrometry. Activity measurement of samples involves the analysis of the peaks in pulse height spectra corresponding to full-energy absorption events based on the number of photons emitted. The peak location is a measure of the photon energy and the peak area of the photon emission rate. For energy measurements the pulse height scale must be calibrated with sources emitting photons of known energies. Two germanium detectors were used for measurement of the samples and have been calibrated with sources emitting photons of known energies (Ba-133, Cd-109, Co-57, Co-60, Cs-137, Mn-54.

Na-22 and Cs/Zn). To compute an emission rate ‘ R ’ for a particular nuclide the detector system must be calibrated with respect to its full energy peak efficiency ‘ ε ’. The emission rate can be obtained from the following equation [19]:

$$R = \frac{N}{T\varepsilon} C1, C2, C3 \quad (12)$$

In above,

N: Number of counts in the full energy peak

T: Measuring time

ε : Full energy peak efficiency

C1, C2, C3: Correction factors

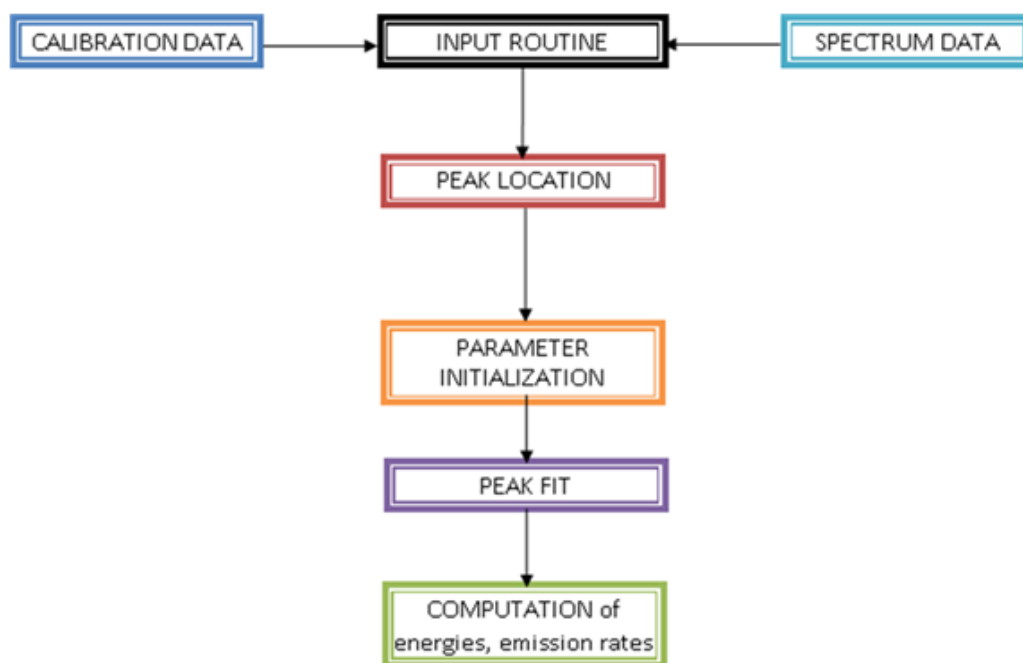


Figure 2.5. Flowchart for Gamma ray Spectrum Analysis

3. ANALYSIS AND IDENTIFICATION OF ELEMENTS

3.1. X-RAY FLUORESCENCE

The X-ray fluorescence measurements were performed (see Fig. 3.1) at the Radiation Measurements and Spectroscopy Laboratory (RMSL) of Missouri S&T Nuclear Engineering department and different types of kidney stones (Apatite, Brushite, Calcium Oxalate Monohydrate 1 & 2, Cystine, Struvite and Uric Acid) were acquired from the Mayo Clinic, Rochester, Minnesota. The schematic of experimental set-up (see Fig. 2.1) includes High Purity Germanium (HPGe) detector, connected to a NIM bin module and then to a computer with Genie 2000 spectroscopy software. The Cd-109 was placed as a radiation source next to the kidney stone on a mounting stand (see Fig. 2.1). The primary fluorescence criterion was considered for identification of the elements. A beam of monochromatic x-rays was incident on the sample. The angle of incidence was 90 degree and the detector was on the same side of the sample and adjacent to the source. To avoid contamination during measurement, forceps with gloves were used to place the sample. The detection geometry was kept same for all kidney stones during counting measurements, and each stone was counted for 30 minutes to get a reliable data. In the present scenario, the characteristics spectral lines emitted by involved elements were used to find the elements and the concentration of the elements. The focus on the $K\alpha$ and $K\beta$ X-ray emissions were considered and elements were then identified (see Fig. 3.2-3.8) [20]. Furthermore, data analysis was performed using the PyMCA open source program [20]. The curve fitting was performed using fitting configuration functions. In order to efficiently run the program several parameters were calculated, optimized and utilized based on the specific detection geometry. In summary, fitting parameters, detector

composition, beam detail, peak information, attenuator description and source flux was utilized to perform the curve fitting operation. The resulting fitted curve was then used to find the elemental concentration and their mass fractions.

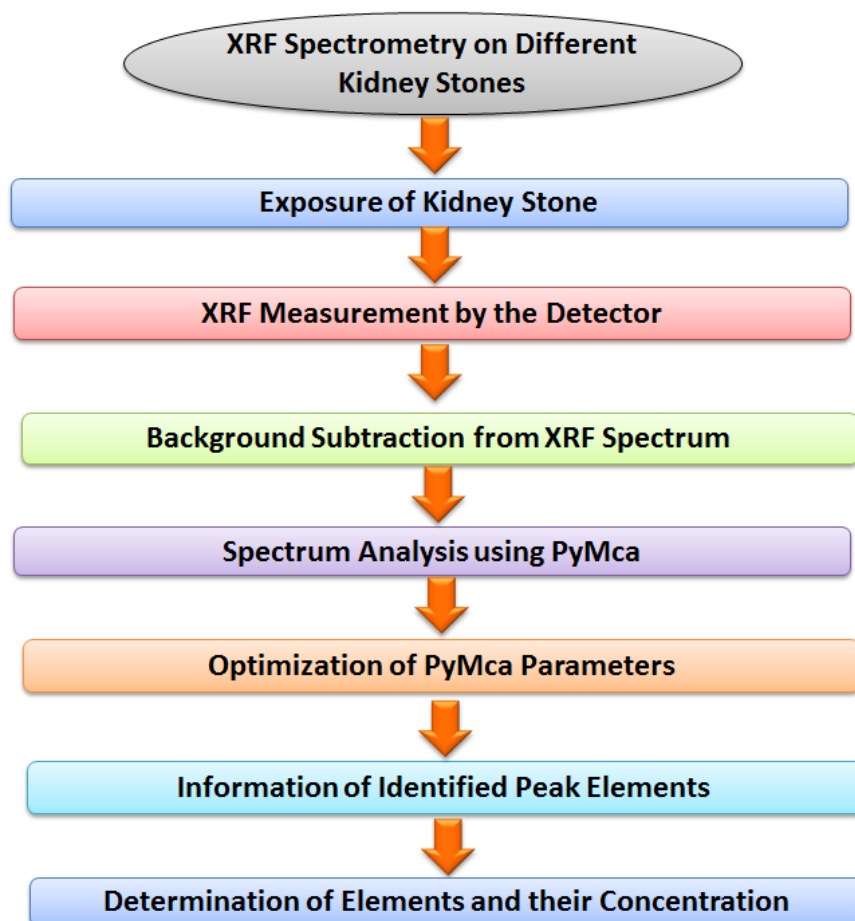


Figure 3.1. Description of XRF Method to Determine the Elements and their Concentration in the Kidney Stones [18]

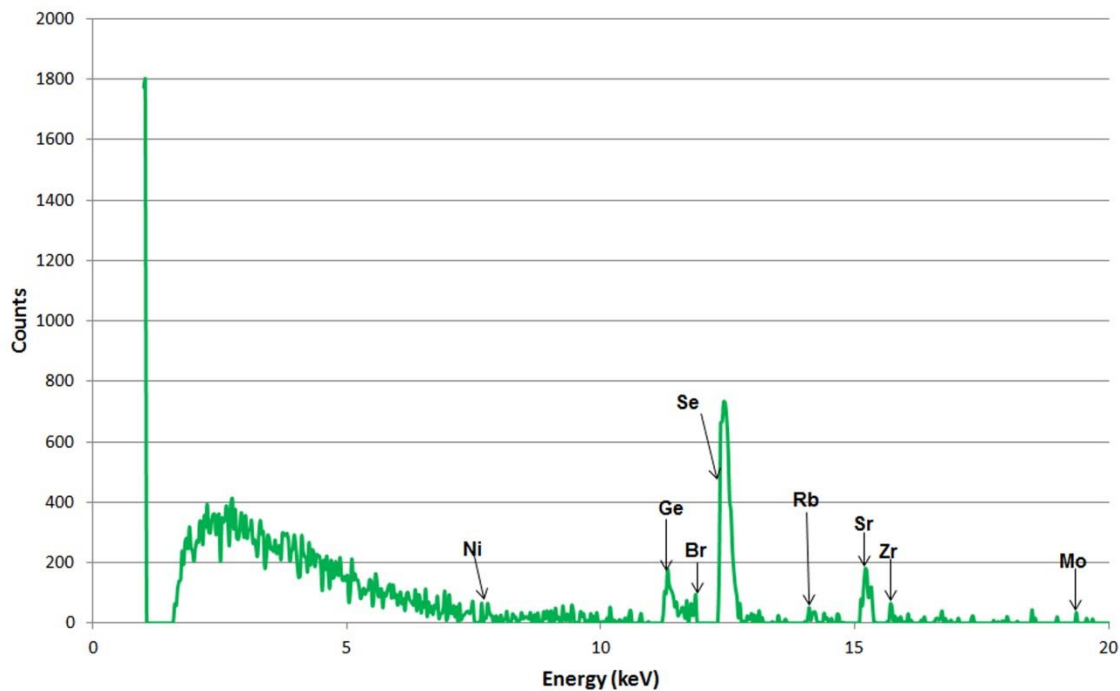


Figure 3.2. XRF Spectrum of the Brushite Kidney Stone

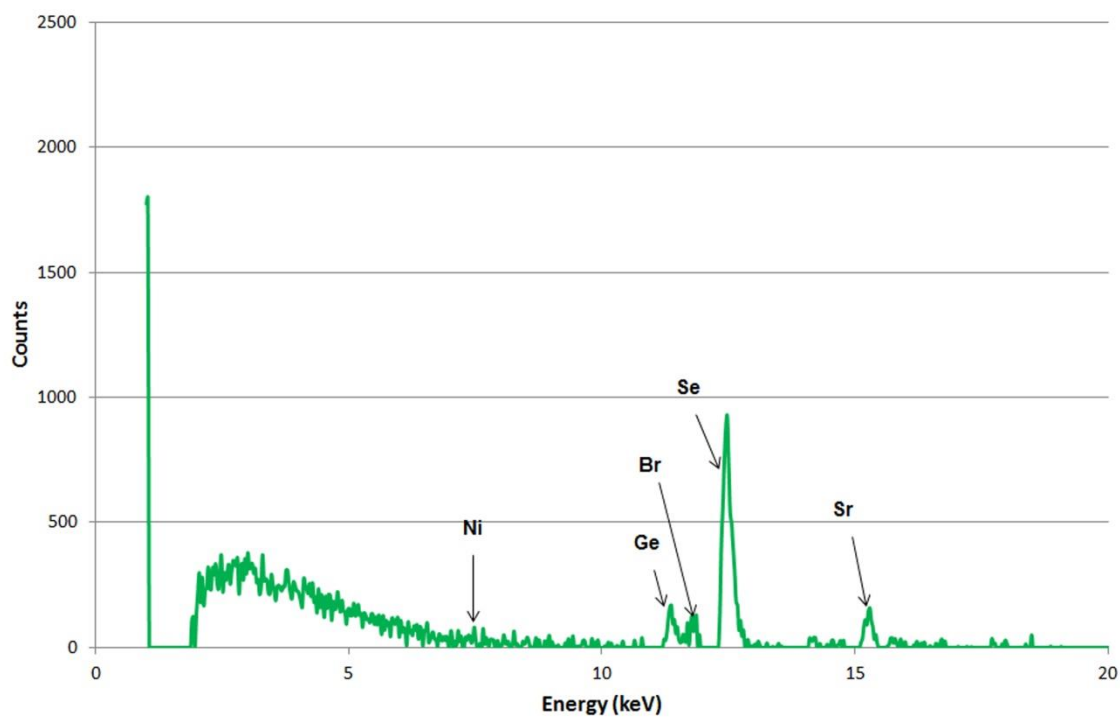


Figure 3.3. XRF Spectrum of the Apatite Kidney Stone

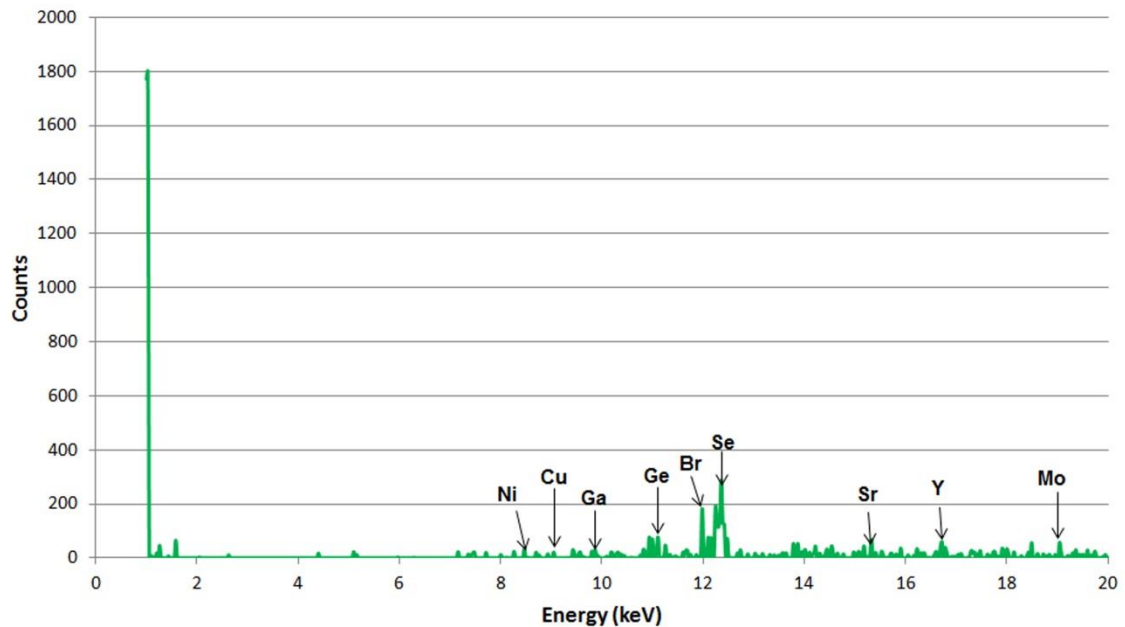


Figure 3.4. XRF Spectrum of the Calcium Oxalate Monohydrate Kidney Stone Sample 1

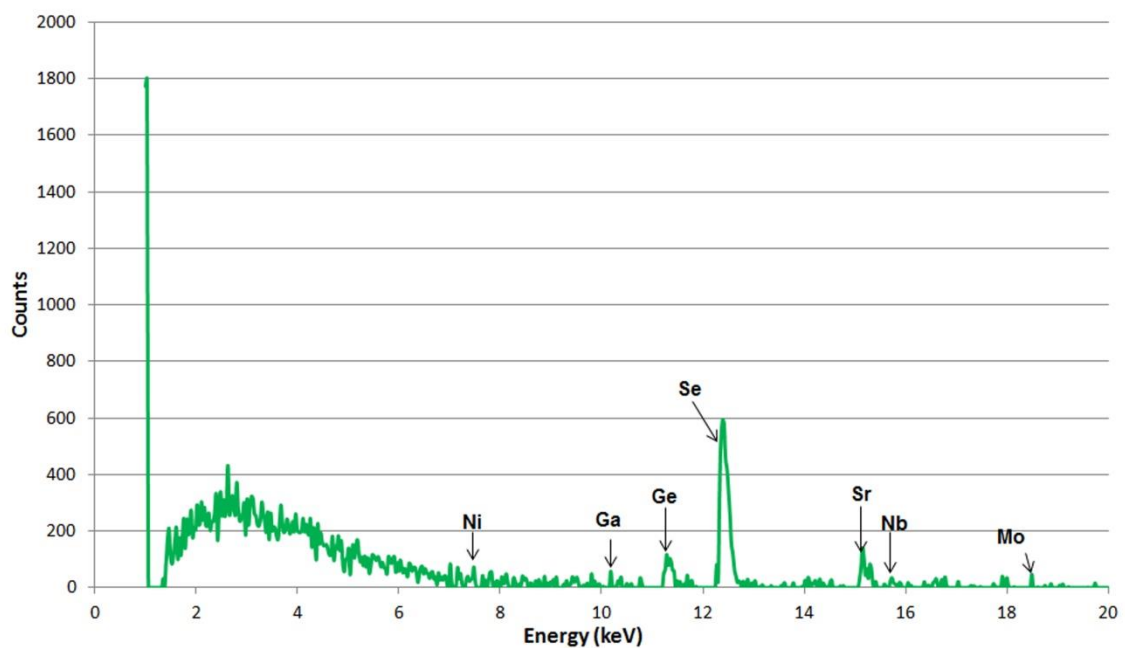


Figure 3.5. XRF Spectrum of the Calcium Oxalate Monohydrate Kidney Stone Sample 2

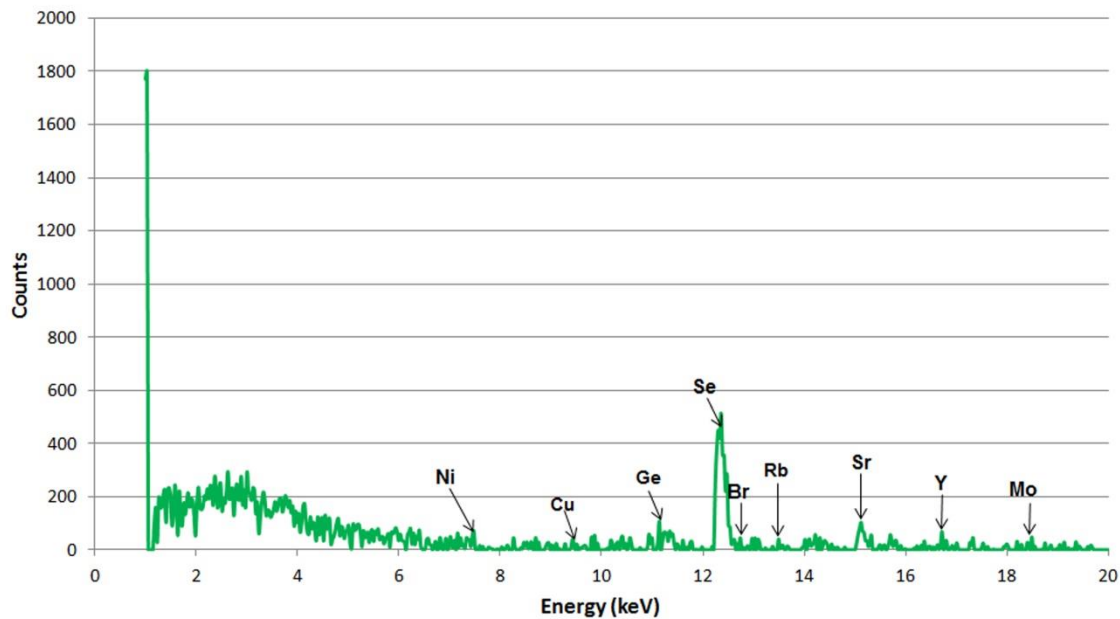


Figure 3.6. XRF Spectrum of the Cystine Kidney Stone

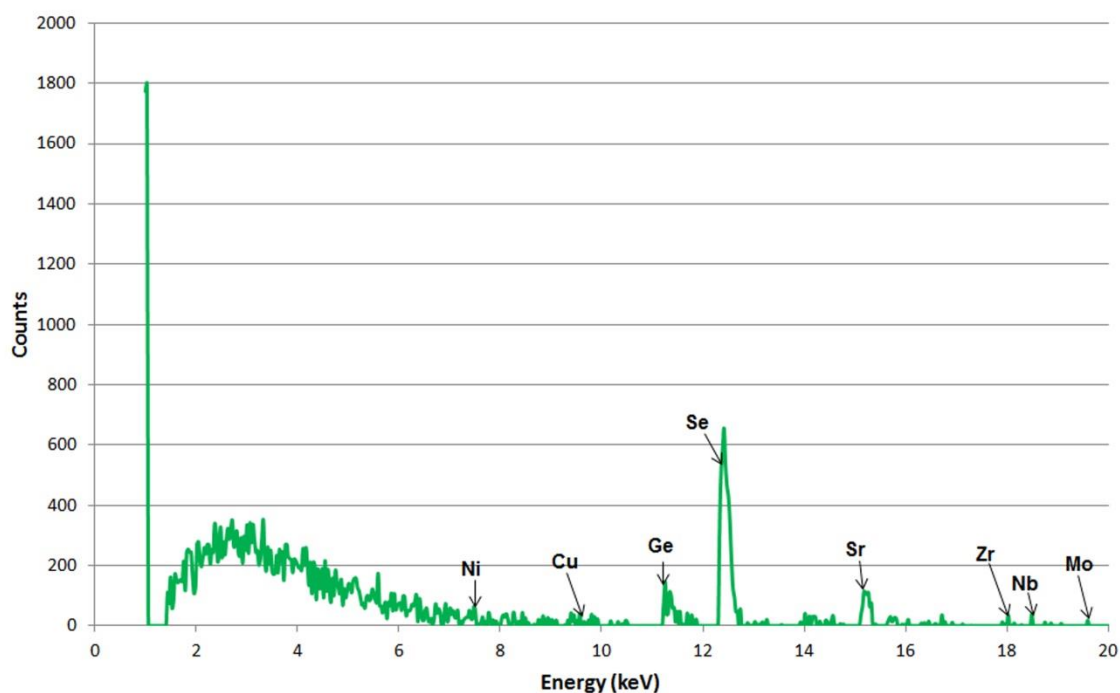


Figure 3.7. XRF Spectrum of the Struvite Kidney Stone

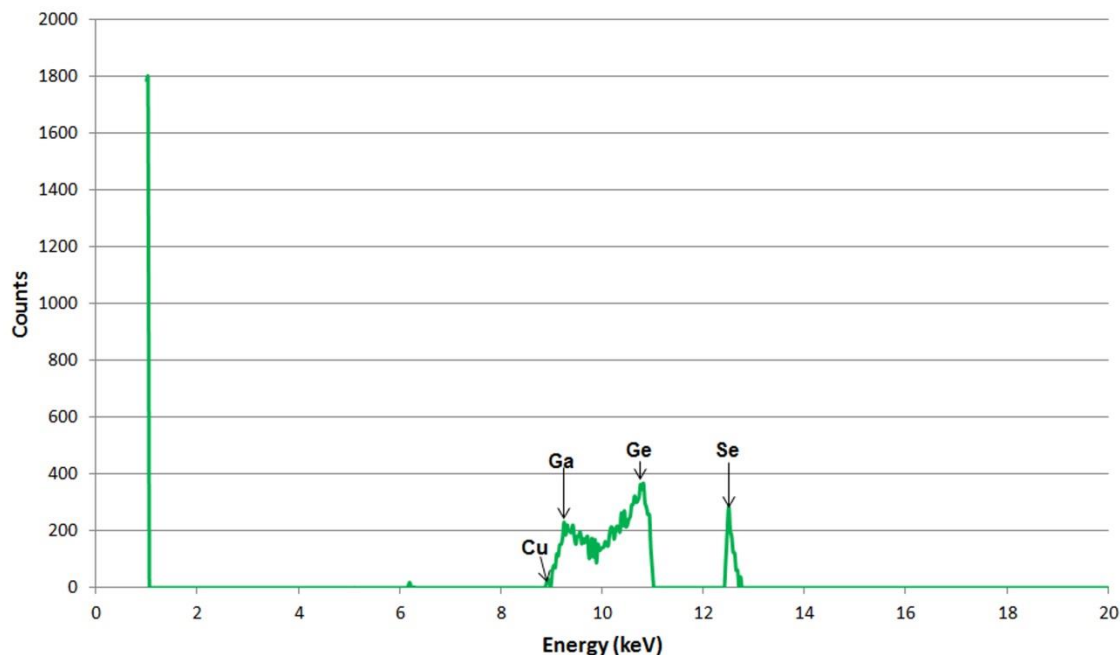


Figure 3.8. XRF Spectrum of the Uric Acid Kidney Stone

3.1.1. Concentration Calculation for XRF Measurements. The relationship between the count rate and mass concentration for each spectral line can be provided by the following equation [21].

$$A = I_0 C \frac{\Omega}{4\pi} \sum_j R_j \quad (13)$$

where I_0 is the incident beam rate, C is the mass fraction of the element in the sample, $\Omega/4\pi$ represents the detector geometric efficiency and R_j is the relative intensity. The incident photon flux, relative intensity and the detector efficiency were used to calculate the mass concentration of the kidney stones. The incident source energy for Cd-109 at 22keV (84%), 25 keV (14%) and 85 keV (4%) was used for the photo excitation. The description of the identified elements peaks for each kidney stone and their concentration is shown (see Table 3.1). The elements which were identified from this techniques are Bromine (Br), Copper (Cu), Gallium (Ga), Germanium (Ge),

Molybdenum (Mo), Niobium (Nb), Nickel (Ni), Rubidium (Rb), Selenium (Se), Strontium (Sr), Yttrium (Y), Zirconium (Zr)

Table 3.1 Relative Concentrations of Kidney Stones from XRF Measurement

Elements	RELATIVE CONCENTRATION (%)						
	Kidney Stones						
	Apatite	Brushite	COM 1	COM 2	Cystine	Struvite	Uric Acid
Ni	0.3162	0.3748	0.3748	0.6644	0.4958	0.1806	-
Cu	-	-	0.07804	-	0.8793	0.071	1.008
Ga	-	-	0.8682	0.1219	-	-	0.2655
Ge	0.79	0.1443	1.843	0.79	0.6558	0.17	0.1876
Se	1.101	0.5038	0.1355	0.4765	3.015	0.193	0.5092
Br	0.08	0.2649	0.1247	-	0.3254	-	-
Rb	-	0.2333	-	-	0.0437	-	-
Sr	0.0575	0.0936	0.03423	0.1991	0.0388	0.006	-
Y	-	-	0.3293	-	0.1091	-	-
Zr	-	0.0199	-	-	-	0.009	-
Nb	-	-	-	0.0198	-	0.003	-
Mo	-	0.008	0.01199	0.0202	0.0075	0.006	-

3.2. NEUTRON ACTIVATION ANALYSIS

NAA experiments were carried out at MSTR (see Fig. 3.9); the kidney stone samples were sent to the reactor by pneumatic transfer system. The samples were irradiated for 3 hr at 100 kW power and then counted on the HPGe detector after 22 hours of decay time. The decay time of 22 hr was sufficient to cool down the sample for an adequate activity. To obtain medium half-life element sample was counted again after 96 hour of decay time. Afterwards, to get a better statistics and reliable data, kidney stone samples were counted for three hours on the HPGe detector. The detection geometry was kept same for all counting experiments. As earlier mentioned in the detector set-up

section, the resulting energy spectrum was analyzed for energy peaks for their corresponding elements (see Fig. 3.10-3.17). The area value under each peak was utilized to calculate the mass of each element found in the kidney stone.

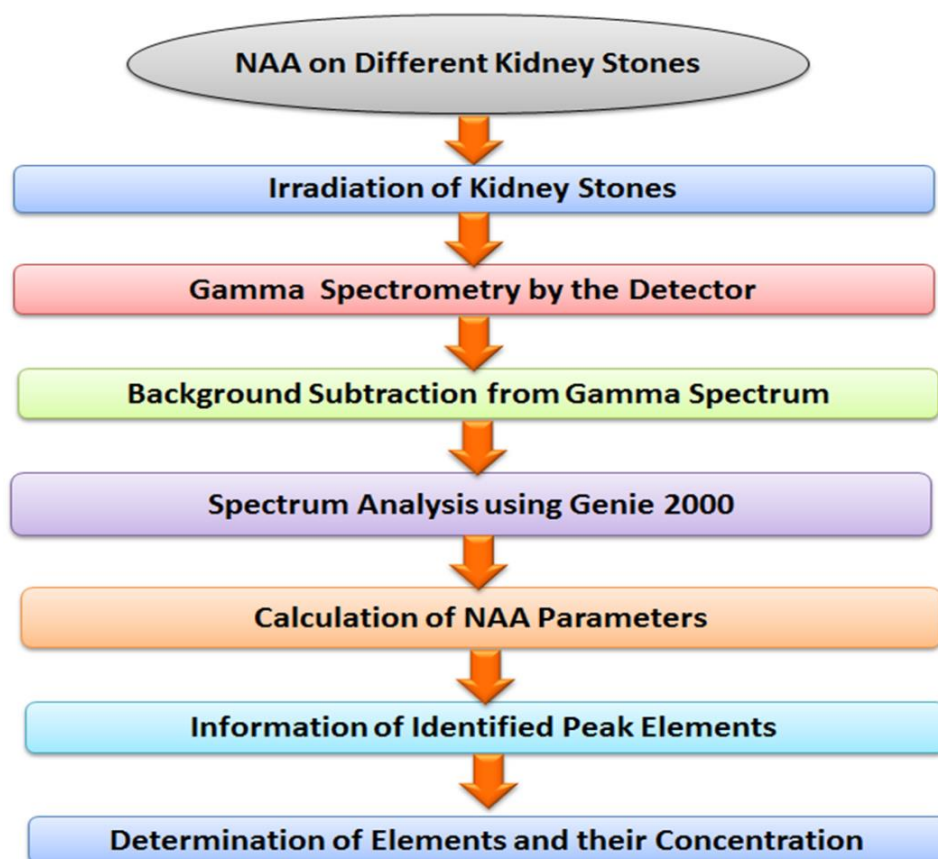


Figure 3.9. Description of NAA Method to Determine the Elements and their Concentration in the Kidney Stones

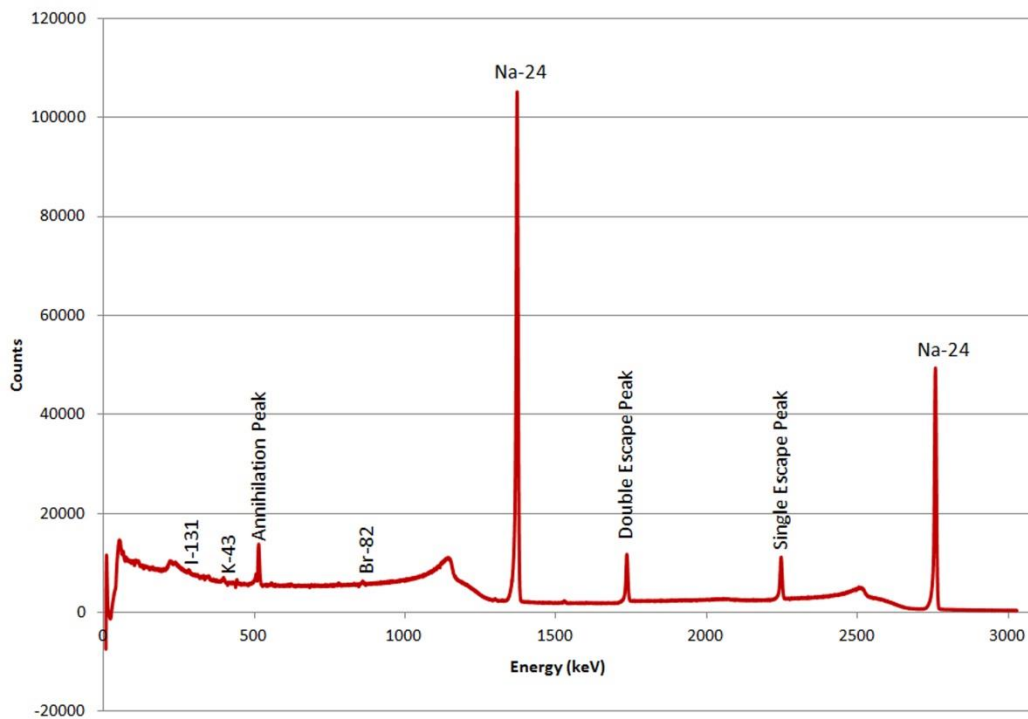


Figure 3.10. Analysis of Apatite Kidney Stone using NAA Method with 3 hrs Counting Time

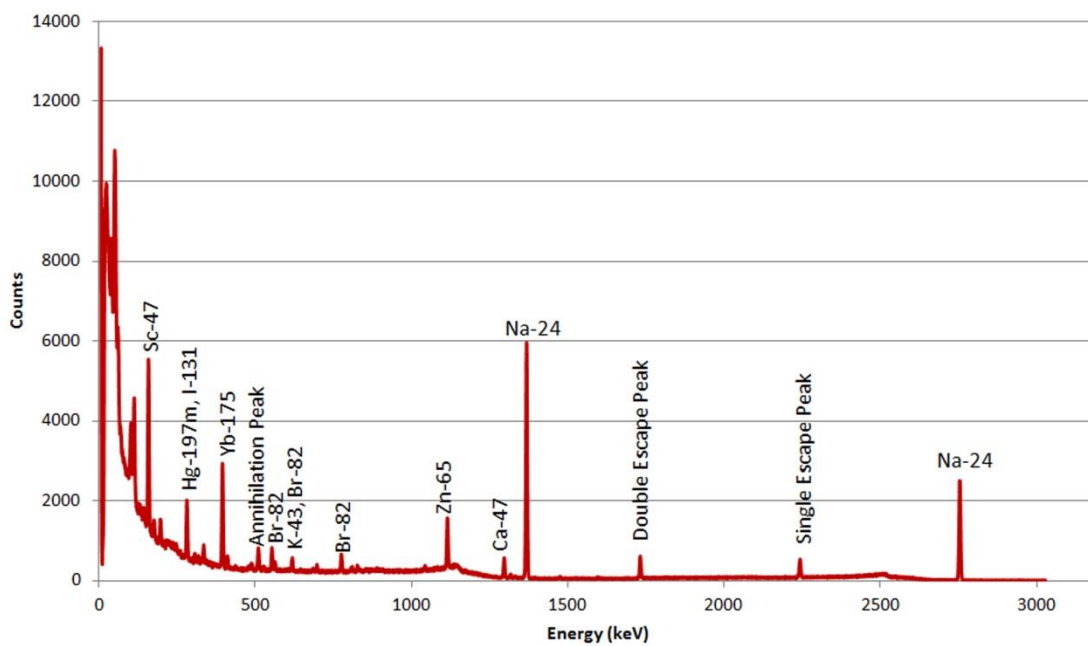


Figure 3.11. Analysis of Apatite Kidney Stone using NAA Method with 8 hrs Counting Time

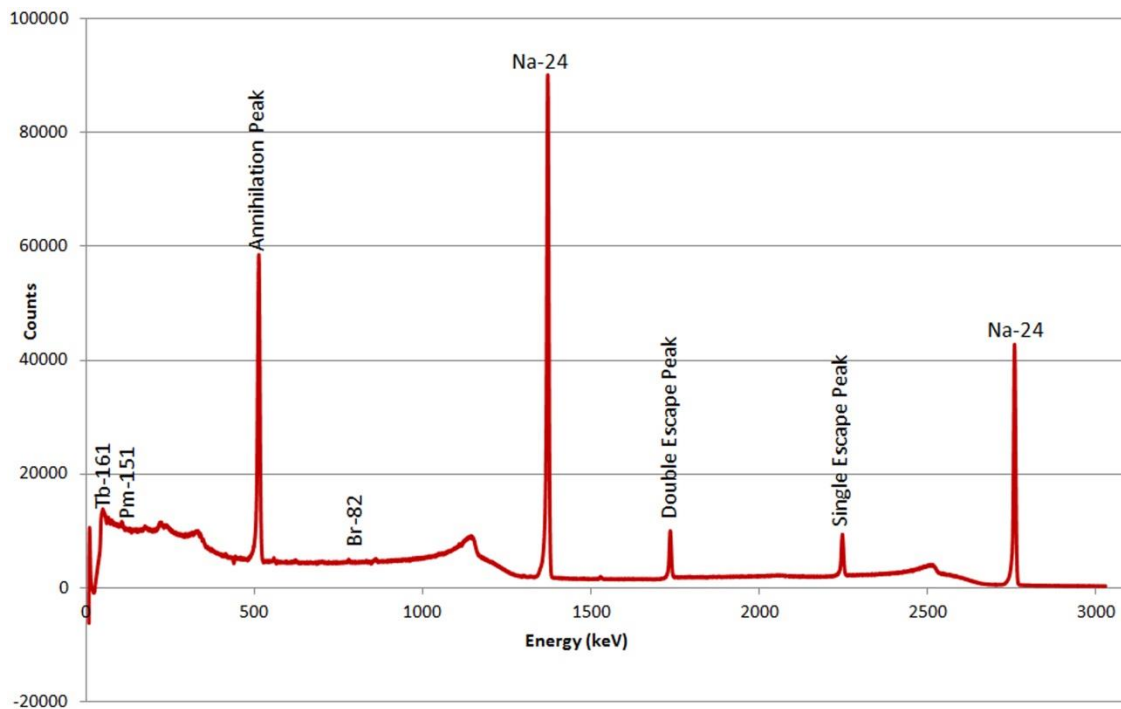


Figure 3.12. Analysis of COM Kidney Stone using NAA Method with 3 hrs Counting Time

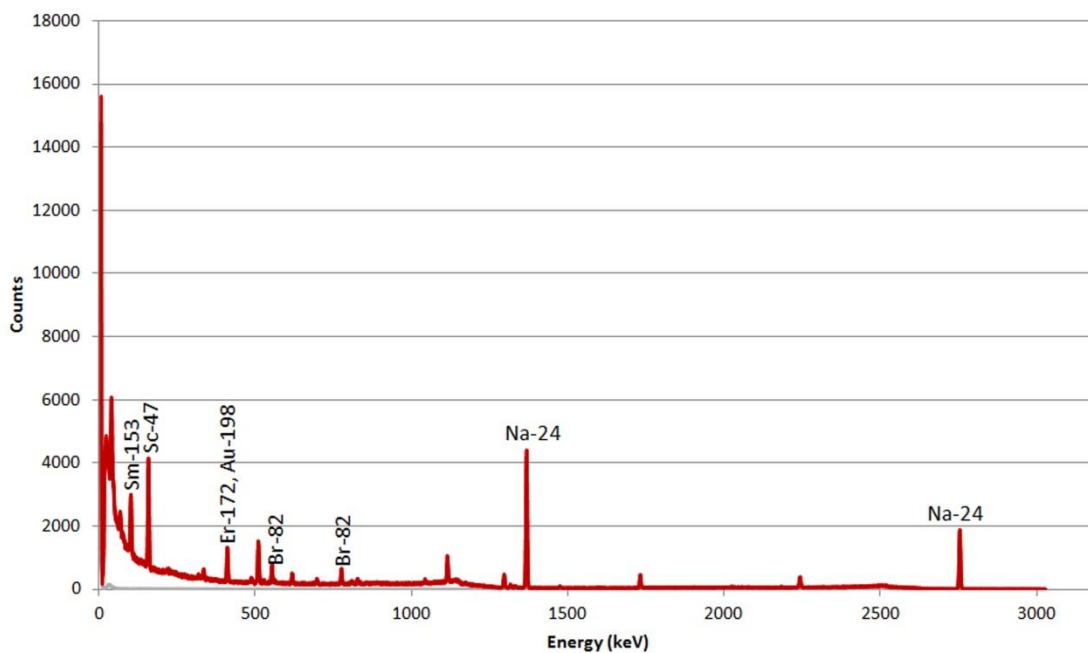


Figure 3.13. Analysis of COM Kidney Stone using NAA Method with 8 hrs Counting Time

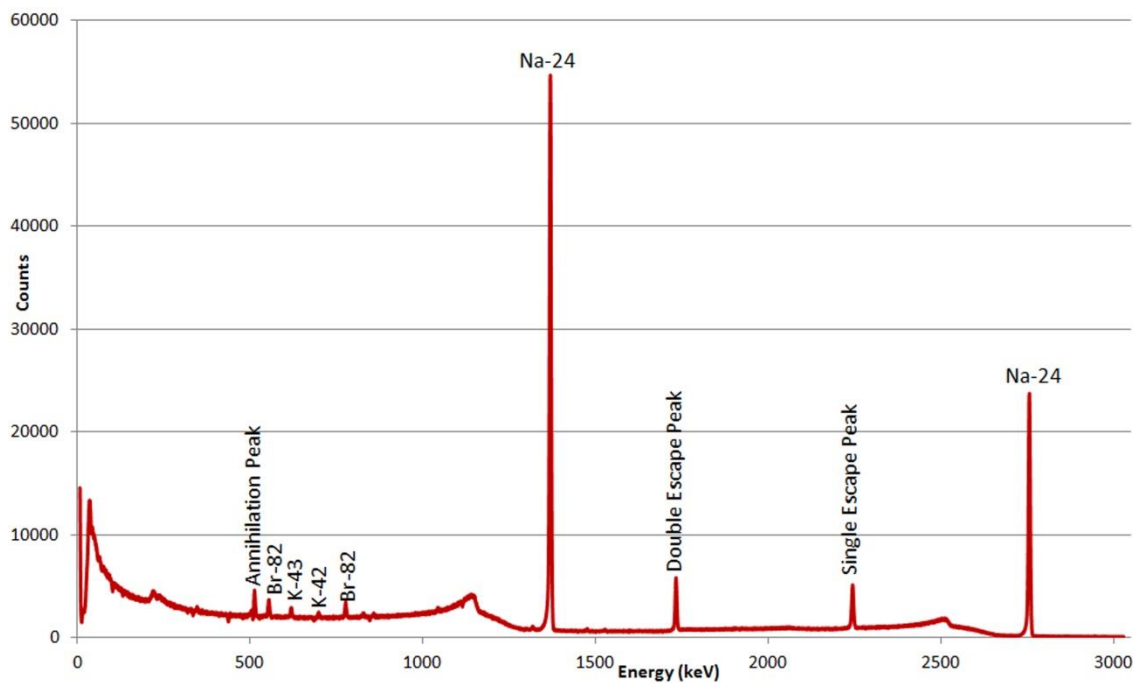


Figure 3.14. Analysis of Struvite Kidney Stone using NAA Method with 3 hrs Counting Time

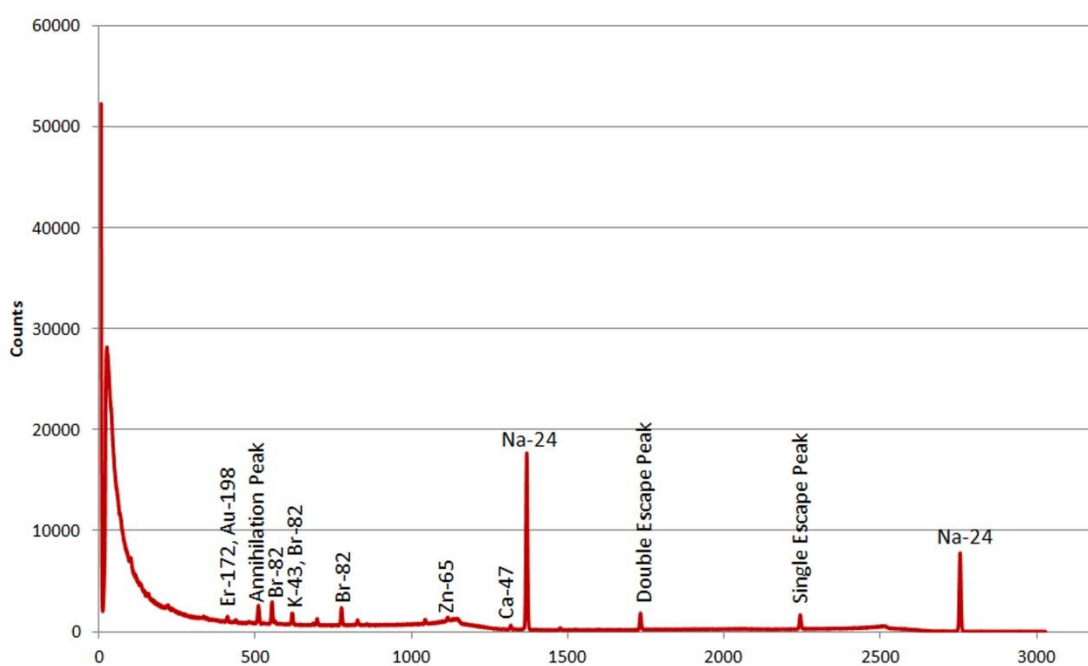


Figure 3.15 Analysis of Struvite Kidney Stone using NAA Method with 8 hrs Counting Time

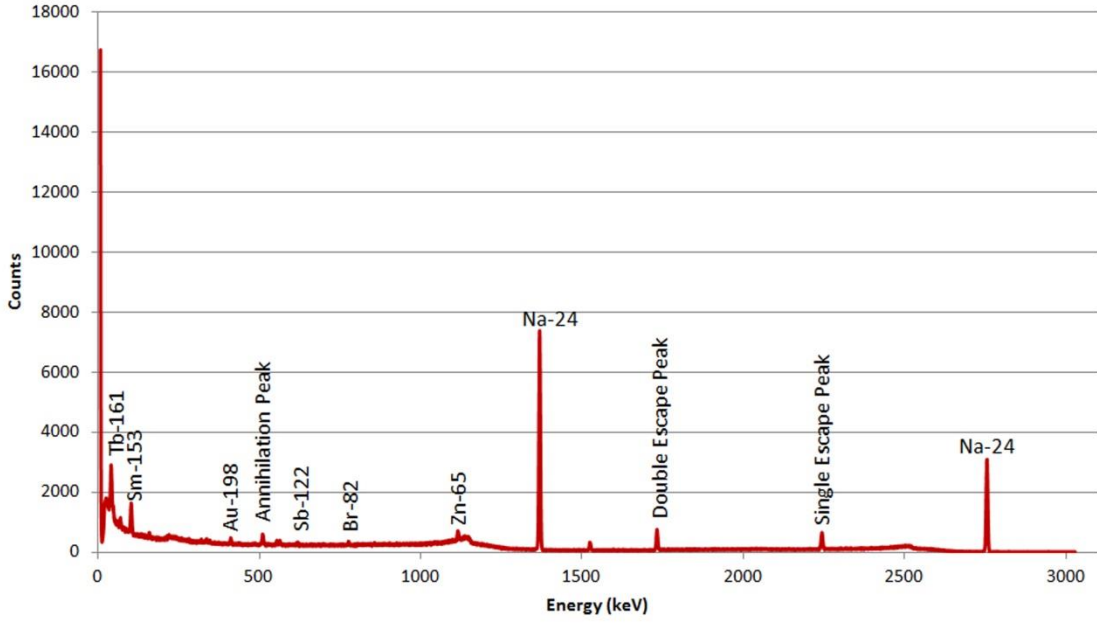


Figure 3.16. Analysis of Uric Acid Kidney Stone using NAA Method with 3 hrs Counting Time

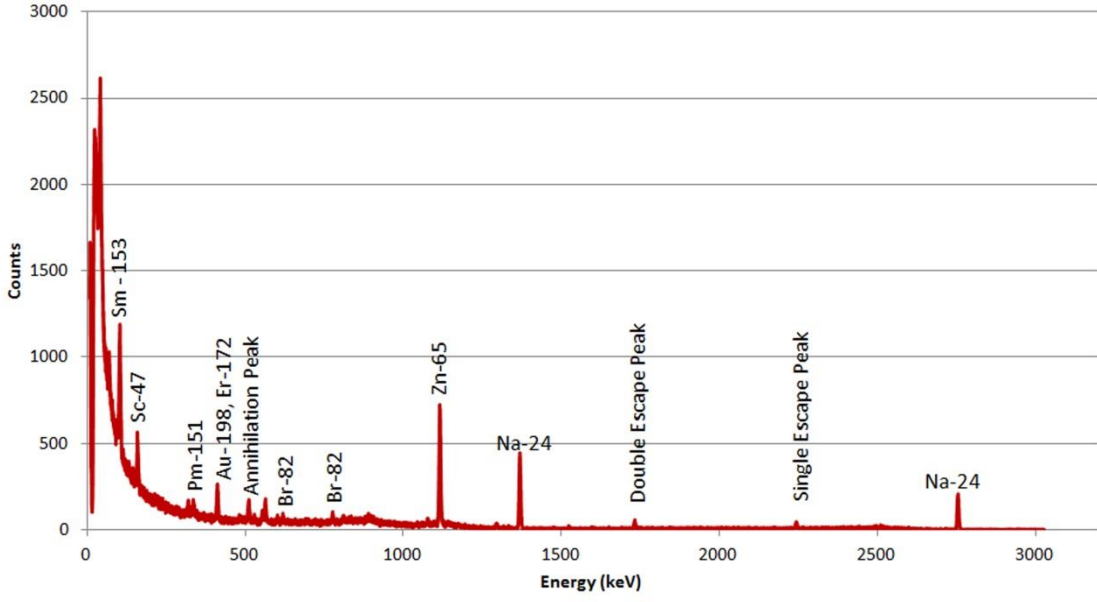


Figure 3.17. Analysis of Uric Acid Kidney Stone using NAA Method with 8 hrs Counting Time

3.2.1. Concentration Calculation for NAA Measurements. The concentration of each element found (see Table 3.2 and 3.3) in the energy spectrum can be related to the mass of original stone by the following equation.

$$M_I = \frac{(Peak\ Area)(A_{rel})}{\phi_{th}\sigma_{th}N_{AV}e^{-\lambda t}} \quad (14)$$

Where M_I is the mass of the radioisotope, *Peak Area* is the area under the energy peak corresponding to the radioisotope, A_{rel} is the molecular weight of the radioisotope, Φ_{th} is the flux value of 4.3×10^{12} n/cm²s, σ_{th} is the thermal cross section of the radioisotope, N_{AV} is Avogadro's Number, λ is the decay constant of the radioisotope, and t is the decay time

Table 3.2 Relative Concentrations of Kidney Stones from NAA Measurement for 3 Hrs Counting Times

RELATIVE CONCENTRATION (%)				
Elements	Struvite	Apatite	COM	Uric Acid
Au	-	-	-	4.11E-12
Br	1.29906E-09	1.67E-09	1.74E-09	8.69E-11
I	-	2.72E-09	-	-
K	2.48218E-09	2.62E-09	-	-
Na	1.13036E-06	3.44E-06	3.8E-06	2E-07
Pm	-	-	1.96E-10	-
Sb	-	-	-	6.16E-14
Sm	-	-	-	1.63E-13
Tb	-	-	1.14E-09	1.6E-10
Zn	-	-	-	1.51E-08

Table 3.3 Relative Concentrations of Kidney Stones from NAA Measurement for 8 Hrs Counting Times

RELATIVE CONCENTRATION (%)				
Elements	Struvite	Apatite	COM	Uric Acid
Au	-	5.55E-11	1.76E-11	4.44E-12
Br	9.45E-09	1.13E-08	8.43E-09	3.11E-10
Ca	1.5E-13	1.61E-13	8.29E-14	-
Er	-	1.86E-11	5.12E-12	1.29E-12
Hg	3.2E-12	-	-	-
I	4.8E-10	-	-	-
K	3.54E-08	3.99E-08	1.65E-08	-
Na	0.000614	0.000591	0.000131	4.44E-06
Pm	-	-	-	9.48E-14
Sc	5.9E-10	5.68E-10	-	3.43E-11
Sm	-	3.1E-12	-	4.13E-13
Yb	8.92E-11	-	-	-
Zn	1.6E-08	1.36E-08	9.23E-09	6.25E-09

4. DISCUSSION AND CONCLUSION

The elements which were identified from XRF techniques are Bromine (Br), Copper (Cu), Gallium (Ga), Germanium (Ge), Molybdenum (Mo), Niobium (Nb), Nickel (Ni), Rubidium (Rb), Selenium (Se), Strontium (Sr), Yttrium (Y), Zirconium (Zr). It is important to mention that observed Germanium (Ge) peak is due to the HPGe detector, which was used for gamma ray spectrometry. The PyMCA open source program is a complete visualization and data analysis tool [4]. The versatility of nonlinear least square fitting incorporated ensures a straightforward integration of the program with the existing experimental setup. The optimization and accurate description of curve fitting functions are essential for the accurate determination of the elements and their concentrations. The experiments were carried out to analyze the composition of kidney stone through X-ray Fluorescence method at the Radiation Measurement and Spectroscopy Laboratory of the Missouri S&T Nuclear Engineering department. The use of PyMCA program to unfold the XRF spectrum is a new approach. It has been shown that present experimental set-up and utilization of open source PyMCA program can serve as an inexpensive tool to identify elemental composition of the kidney stones and their concentration with a high degree of accuracy. Furthermore, the elements which were identified from NAA techniques are Gold (Au), Bromine (Br), Calcium (Ca), Erbium (Er), Mercury (Hg), Iodine (I), Potassium (K), Sodium (Na), Promethium (Pm), Antimony (Sb), Scandium (Sc), Samarium (Sm), Terbium (Tb), Ytterbium (Yb), Zinc (Zn). The simple analytical equation was utilized for determination of mass concentration of identified element in the kidney stone sample. The results from combined use of XRF and NAA analysis can serve as a reliable method to accurately determine the elemental composition of the

kidney stones. Furthermore, the elements Sodium (Na) and Bromine (Br) were detected by both techniques and consistent with the identified elements in terms of linear attenuation coefficients and thermal total cross-sections values. The combined use of XRF and NAA experiments provide a comprehensive analysis of the kidney stone compositions. The application of both techniques (XRF and NAA) on the kidney stone samples provide a mean to detect all possible minor and trace elements involved in composition of a kidney stone sample. The research results could be a valuable addition to the existing research database for elementals analysis of the various types of kidney stones. Certainly, identified elements in the kidney stone depends on the dietary habits and environmental location of the patients. Therefore, presence of different elemental composition in each stone can be accounted due to the same cause. The results from such analysis can be utilized from physicians and researchers to develop more effective methods to develop the new medicines for kidney stones. In future work, more experiments can be carried out with different radioisotope sources and flux values for XRF and NAA experiments. Additionally, other elemental analysis techniques can be parallel performed to provide a more comprehensive analysis and can be compared with XRF and NAA results.

APPENDIX.

Calibration Information for HPGe Detector at MSTR

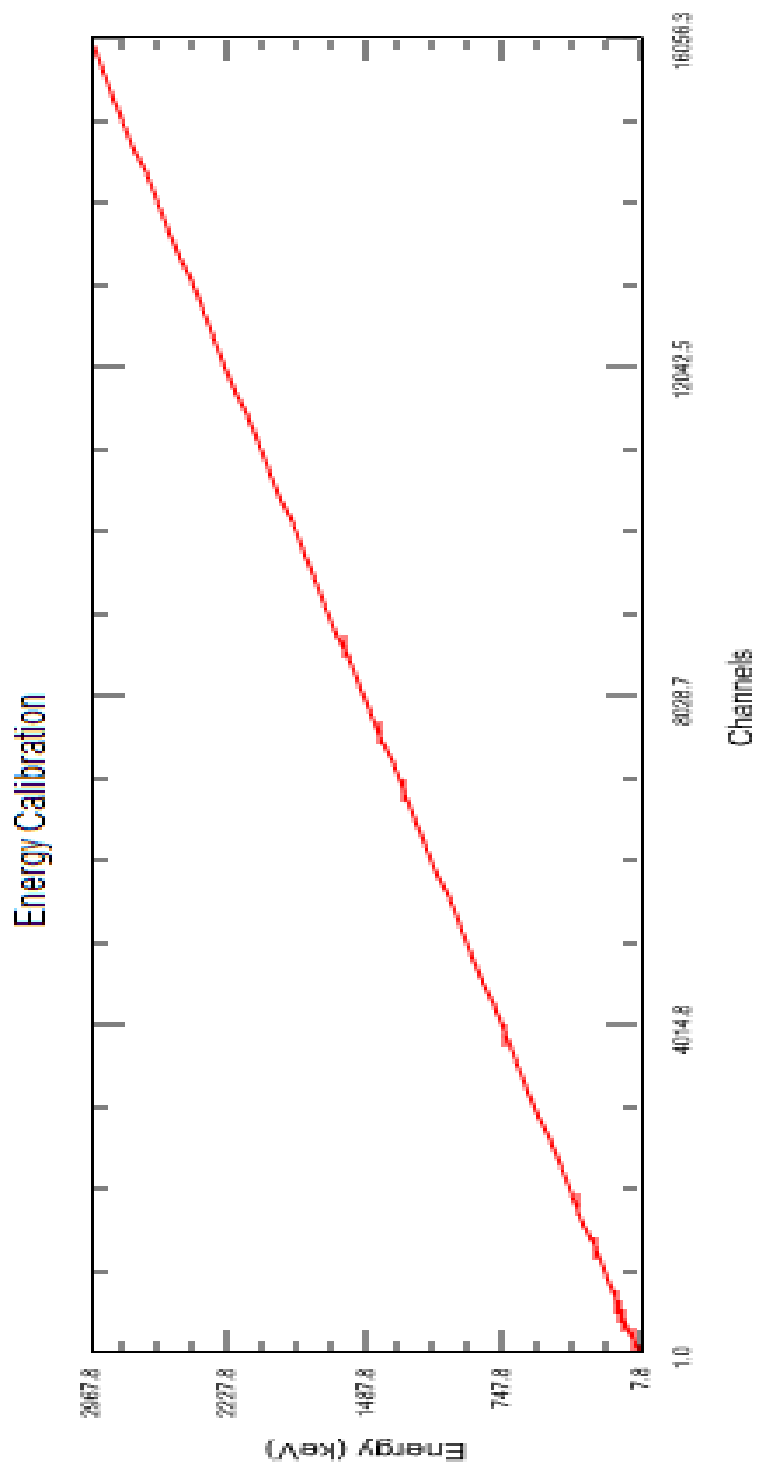


Figure A.1 Energy Calibration

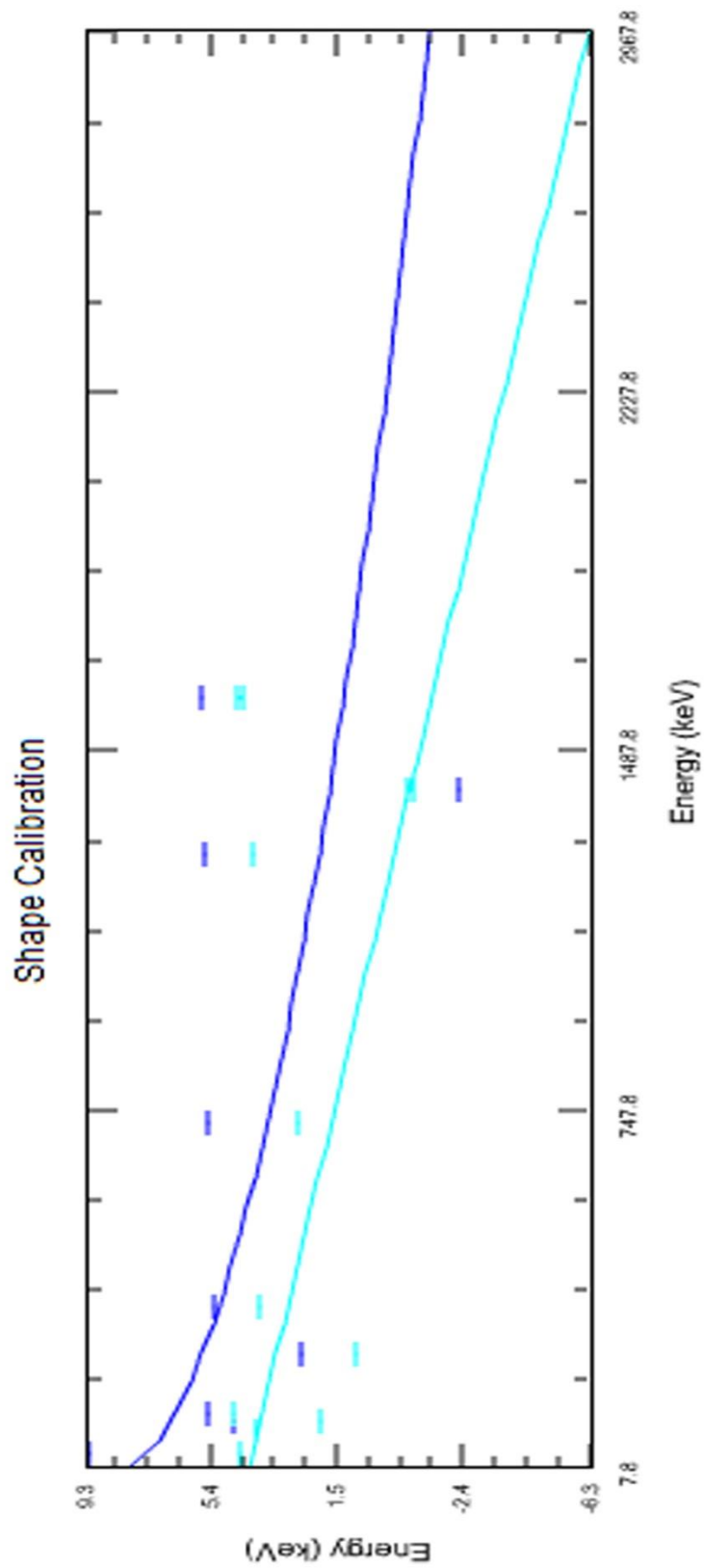


Figure A.2 Shape Calibration

Table A.1 Calibration Information for HPGe Detector at MSTR

	a		b	c	χ^2
Energy	7.647	+	0.184 Ch		1.462e6
FWHM	8.432	+	-0.180 E		1.167e6
Low Tail	4.198	+	-3.542e-3 E		9.046e4

BIBLIOGRAPHY

- [1] Romero V., Akpınar H., Assinos D.G., Kidney Stones: a global picture of prevalence, incidence, and associated risk factors, *Reviews in Urology*, 2010, Vol. 12, pp. 86-96.
- [2] Hamos, L. V., *Arkiv för Matematik, Astronomi och Fysik*, 1945, Vol. 31A.
- [3] Sherman, J., ASTM Special Technical Publication No. 157, 1954, pp. 27–33.
- [4] Sherman, J., The theoretical derivation of fluorescent X-ray intensities from mixtures, *Spectrochimica Acta*, 1955, Vol. 7, pp. 283–306.
- [5] Rousseau R.M., Corrections for matrix effects in X-ray fluorescence analysis—A tutorial, *Spectrochimica Acta Part B: Atomic Spectroscopy*, July 2006, Doi:10.1016/j.sab.2006.06.014, pp. 759-777.
- [6] Heggie, J. C., Liddell, N. A., Maher, K. P. *Applied Imaging Technology*, 4th Edition, St. Vincent's Hospital Melbourne, 2001.
- [7] Tsoufanidis N., *Measurement and Detection of Radiation*, Taylor and Francis Group, Boca Raton, FL, U.S., 1995, pp. 153-175.
- [8] Knoll G. F., *Radiation Detection and Measurement*, 2nd Edition, Wiley Publishers, 0-471-81504-7, 1989, pp. 50-54,365.
- [9] Jenkins R., *X-Ray Fluorescence Spectrometry*, Wiley-Interscience, Hoboken, NJ, 1999.
- [10] <http://digitalcommons.mcmaster.ca/opendissertations/7266/>, Moldovan N., *Measurement of Transition Metals in the Rodent Brain using X-Ray Fluorescence and Neutron Activation Analysis*, McMaster University, Ontario, 2012 (Accessed September 1st, 2013).
- [11] <http://www.horiba.com/us/en/scientific/products/x-ray-fluorescence-analysis/tutorial/x-ray-fluorescence-intensity/>, *X-Ray Fluorescence - Intensity*, HORIBA International Corporation, Japan, 1996-2014 (Accessed September 1st, 2013).
- [12] Wolbrast A. B., *Physics of Radiology*, Medical Physics Publishing Corporation, 2005.
- [13] <https://mospace.umsystem.edu/xmlui/handle/10355/41197>, Sinha V., *Design, development and characterization of a novel neutron and X-ray combined computed tomography system*, Missouri University of Science and Technology, Rolla, 2013 (Accessed March 20th, 2014).

- [14] http://archaeometry.missouri.edu/naa_overview.html, Glascock, D. M., Overview of Neutron Activation Analysis. Missouri University Archaeometry Laboratory, Columbia, 2010. (Accessed March 15th, 2014).
- [15] <http://atom.kaeri.re.kr/cgi-bin/endlplot.pl>, Los Alamos National Laboratories: ENDF/B-6.1 mat2843. Cross Section Plotter. Korea Atomic Energy Research Institute (Accessed April 6th, 2014)
- [16] Lockheed Martin. Nuclides and Isotopes - Chart of the Nuclides. 16th. s.l.: Knolls Atomic Power Laboratories, 2002. pp. 46-47.
- [17] Pollard, A. M., Heron C., Archaeological chemistry, 2nd Edition, Cambridge: Royal Society of Chemistry, 1996.
- [18] Srivastava A., Heisinger B. J., Sinha V., Lee H. K., Liu X., Qu M., Duan X., Leng S., McCollough C. H., Determination of minor and trace elements in kidney stones by x-ray fluorescence analysis, Proc. SPIE 9033, Medical Imaging, March 2014, doi: 10.1117/12.2043733.
- [19] Debertin K., Helmer R. G., Gamma- and X-Ray Spectrometry with Semiconductor Detectors, 3rd Edition. North Holland, 1988.
- [20] Pemmer B., Roschger A., Wastl A., Hofstaetter J.G., Wobrauschek P., Simon R., Thaler H.W., Roschger P., Klaushofer K., Strelci C., Spatial distribution of the trace elements zinc, strontium and lead in human bone tissue, Bone, August 2013, Vol. 57(1), pp. 184-193.
- [21] Solé V. A., Papillon E., Cotte M., Walter Ph., Susini J., A multiplatform code for the analysis of energy-dispersive X-ray fluorescence spectra, Spectrochimica Acta Part B: Atomic Spectroscopy, January 2007, Vol. 62(1), pp. 63-68.

VITA

Anjali Srivastava was born in Allahabad, India. In the year 2004, she received her Bachelor's degree in Computer Applications from M.C.R.P University Bhopal, India. She graduated with a Master's degree in Computer Applications from U.P. Technical University, Lucknow, India in the year 2006. She worked as a System Administrator at the Reliance Communications Limited India. She has also participated in different research projects at the Missouri University of Science & Technology in the areas of design and development of a novel neutron and X-ray combined computed tomography system and Monte Carlo Simulation of a Bowtie Filter. She obtained her Master of Science degree in Nuclear Engineering from Missouri University of Science & Technology in August 2014. She has performed her Master's thesis in determination of minor and trace elements in kidney stone using XRF and NAA techniques. She has authored 4 peer reviewed conference proceeding articles and 2 journal articles while working for her master's degree at the Missouri University of Science & Technology. She was inducted into Alpha Nu Sigma nuclear engineering honor society in 2013. She is a member of American Nuclear Society (ANS) and Council on Ionizing Radiation Measurements and Standards (CIRMS). In recognition of her research, she has also received the CIRMS student award of 2013-2014 at the National Institute of Science & Technology.

